AFIT/GA/ENY/97D-05

DEVELOPMENT AND VALIDATION OF AN EXPERIMENTAL TEST RIG FOR ELECTROHYDRODYNAMIC ENHANCEMENT OF FORCED CONVECTIVE HEAT TRANSFER

THESIS

William T. Caldwell, Captain, USAF

AFIT/GA/ENY/97D-05

AFIT/GA/ENY/97D-05

DEVELOPMENT AND VALIDATION OF AN EXPERIMENTAL TEST RIG FOR ELECTROHYDRODYNAMIC ENHANCEMENT OF FORCED CONVECTIVE HEAT TRANSFER

THESIS

Presented to the Faculty of the Graduate School of Engineering of the

Air Force Institute of Technology

Air University

Air Education and Training Command

In Partial Fulfillment of the Requirements for the

Degree of Master of Science in Astronautical Engineering

William T. Caldwell, B.S.

Captain, USAF

December 1997

AFIT/GA/ENY/97D-05

DEVELOPMENT AND VALIDATION OF AN EXPERIMENTAL TEST RIG FOR ELECTROHYDRODYNAMIC ENHANCEMENT OF FORCED CONVECTIVE HEAT TRANSFER

William T. Caldwell, B.S.
Captain, USAF

Approved:

Chairman	17 Feb '98 date
	24 Feb 98 date
	2 Mar 98 date

The views expressed in this thesis are those of the author and do not reflect the official policy or position of the Department of Defense or the U.S. Government.

Acknowledgments

The nature of this project required me to reach out to many individuals for their guidance, expertise, and support. I am better for having been involved with such individuals, and have been strengthened by their talents.

I would like to express my sincere appreciation to my faculty advisor, Maj. Jeffery Little for his guidance and patience throughout this effort.

I am especially indebted to the TATLAB and AFRL/VAVE professionals whose willingness to share their experience and guidance enabled me to have a strong educational experience. Many thanks to Dr. David Pratt, Lt. John Paschkewitz, and SSgt John Williams for their patient tutelage and tireless dedication to this project. A special thanks goes to Jack Holliday and the other T/SSI professionals for sharing their expertise and for putting up with me underfoot. I have learned a great deal from you all.

Above all others, my greatest appreciation is reserved for my wife, Cami, whose unwavering love, understanding, and sacrifice allowed me to focus on this program.

William T. Caldwell

Table of Contents

Page

Acknowledgements iii

List of Figures vi

List of Tables vii

List of Symbols viii

Abstract x

I. Introduction 1

1.1 Background 1
1.2 Problem Statement 5
1.3 Summary of Current Knowledge 6
1.4 Objective and Scope 9
1.5 Methodology 10

II. Theory 13

2.1 Hydrodynamics 13
2.2 Maxwell's Equations 15
2.3 EHD Bulk Force Density 16

III. Experimental Setup 23

3.1 Test Loop 23
3.1.1 Design Criteria / General Description 23
3.1.2 Fluid Control and Flow Measurement 26
3.1.3 Fluid Temperature Maintenance 30
3.1.4 High and Low Voltage Support 33
3.1.5 Temperature and Pressure Measurement 34
3.1.5.1 Differential Thermocouple 34
3.1.5.2 Absolute and Differential Pressure Transducers 38
3.2 Contamination Control 40
3.3 Data Acquisition System 42

3.4 Test Section 44
3.5 Loop Validation Tests 46
3.5.1 Fluid Choice / Pool Fluid Extraction 47
3.5.2 Leak Checks 50
3.5.3 Loop Temperature Settling Time 51
3.5.4 EHD Sparkover Voltage 51
3.5.5 Low Voltage Telemetry Sensitivity 52

IV. Results and Discussion 56

4.1 Test Rig Anomalies, Troubleshooting, and Resolutions 56
4.1.1 Data Acquisition System 56
4.1.2 Flow Generation and Measurement 58
4.1.3 Contamination Control 60
4.1.4 Test Section 62
4.2 Data Set Description 64
4.3 Data Reduction 66

V. Conclusions 73

Appendix A: ERROR ANALYSIS A-1

Appendix B: CALIBRATION DATA B-1

Appendix C: FLUID PROPERTIES C-1

Appendix D: MASS FLOW AND REYNOLDS NUMBER CALCULATIONS D-1

Appendix E: PROCEDURAL NOTES E-1

Bibliography Bib-1

Vita Vita-1

List of Figures

Figure		Page
1	Secondary Flow Generated by Corona Wind	4
2	Behavior of Charged and Neutral Molecules in a Uniform Electric Field	19
3	Behavior of Charged and Neutral Molecules in a Non-Uniform Electric Field	21
4	Experimental Test Rig Schematic	25
5	Process Fluid Loop - Test Section End	25
6	Coriolis Flowmeter	30
7	Magnetic Gear Pump	30
8	Process Fluid Heat Exchanger	32
9	Theoretical Basis for a Simple Differential Thermocouple	35
10	Standard E-type and Constructed Differential Thermocouple	36
11	Differential Thermocouple Calibration Setup	37
12	Pressure Transducer Calibration Setup	39
13	Data Acquisition System Overview	42
14	Heat Transfer Test Section	45
15	Pool Fluid Extraction Test	48
16	Set A - Heat Input Validation	68
17	Set A - Differential Pressure vs. Heat Input	68
18	Set A - Absolute Pressure vs. Heat Input	68
19	Sets B & C - Differential Temperature vs. EHD Voltage	69
20	Sets B & C - Differential Pressure vs. EHD Voltage	69
21	Sets B & C- Absolute Pressure vs. EHD Voltage	69

List of Tables

Table		Page
1	Pump Head Flow Rate Ranges	29
2	Results of Pool Fluid Extraction Test	49
3	Description of Modified Data Sets	65
4	Error Analysis Summary	70

List of Symbols

Symbol	Description	Units
A_c	Heat transfer channel cross sectional area	m^2
c_p	Fluid specific heat	J/kg•K
d	Electrode separation	m
d_h	Nichrome heater wire diameter	m
D_h	Heat transfer channel hydraulic diameter	m
$\overline{E}$	Electric field strength	V/m
f_e	Electrohydrodynamic body force density	N/m^3
F_p, $\overline{F}_P$	Force on a charge particle	N
g	Acceleration of gravity	m/s^2
$\dot{m}$	Mass flow rate	kg/sec
p	Fluid pressure (absolute)	N/m^2
$\overline{J}$	Electric current density	C/m^2•s
q_p	Particle charge	C
R_h	Heater resistance	ohm
Re	Reynolds number	
T	Fluid temperature	°K, °C
t	Time	sec
$\overline{u}$	Mean fluid velocity	m/sec
$\dot{V}$	Volumetric flow rate	m^3/sec
VDC	Direct current voltage	V

VAC	Alternating current voltage	V
ΔT	Differential temperature	^{o}K, ^{o}C
P1A	Absolute pressure channel descriptor	
P2D	Differential pressure channel descriptor	
EHD	ElectroHydroDynamics	
α	Fluid thermal diffusivity	m^2/sec
ε	Dielectric permittivity	F/m
ϕ	Electric potential	V
κ	Dielectric constant ($\varepsilon/\varepsilon_o$)	
μ	Fluid dynamic viscosity	$N \cdot s / m^2$
ρ	Fluid Density	kg/m^3
ρ_c	Fluid free/space charge density	C/m^3
σ_e	Fluid electrical conductivity	$1/ohm \cdot m$

Abstract

This report details the development of a facility for the experimental investigation of electrohydrodynamic (EHD) enhancement of forced convection heat transfer. The test facility was developed for the Thermal and Transparencies Laboratory (TATLAB), Air Force Research Laboratory (AFRL), for use in future research into the applicability of EHD for the miniaturization of Air Force heat exchangers.

During this research, a closed loop, medium scale electrohydrodynamic test rig was developed and brought online. The test fluid loop was integrated with a data acquisition and parameter control system. Basic loop and fluid performance testing was accomplished through the use of a 3mm hydraulic diameter, square channel test section using Flourinert FC-72, a dielectric electronics coolant, as the working fluid.

Due to the design of the test section, no heat transfer data was generated in this initial study. However, this study greatly expanded the experimental and practical understanding of the EHD phenomenon within AFRL, by providing a working knowledge of the basics of effective EHD test section design, contamination control procedures, and loop design and operation. Deficiencies in the design of the loop, data acquisition system, and test section were identified and recommendations for improvements in future work were delivered. The Air Force Research Laboratory is now poised to generate useful EHD heat transfer data with this test facility.

DEVELOPMENT AND VALIDATION OF AN EXPERIMENTAL TEST RIG FOR ELECTROHYDRODYNAMIC ENHANCEMENT OF FORCED CONVECTIVE HEAT TRANSFER

I. Introduction

1.1. Background

The technological nature of the United States Air Force has historically driven it to seek those technologies that enhance the capabilities of existing systems and give developing systems a marked advantage over those of the competing forces. Any such technology that improves a system's central design budgets of size, weight, and power has the potential to provide just such an advantage. For an air and space force, the overall performance of an airborne system is directly tied to its design efficiency, or the percent size, weight, or power of the total system that is dedicated to payload. This efficiency is increased when a critical parameter of one of the support systems is improved, thereby increasing the amount of the budget available for payload augmentation.

Environmental control systems, while critical to the support of any airborne platform, generally take up a sizable portion of the support system budget. This is particularly true when humans are part of the cargo. As the Air Force continues to push the technology envelope in the form of higher performance aircraft and space launch systems, the associated propulsion systems will be required to perform in a more intense thermal environment. This

will, in turn, generate a need for higher capacity thermal handling equipment on board these systems. Also, on a smaller scale, the continuing increase in reliance on higher speed computers as the basis for advanced avionics systems will call for exponentially increasing electronic cooling capability. The bottom line is this: the demand on thermal protection and conditioning subsystems will undoubtedly increase in the near future.

In the last 40 years, there has been a substantial amount of effort put forth by industry and government to develop single- and two-phase compact heat exchangers, those devices having a large internal surface area density. This topic is well covered in the classic text by Kays and London [11]. While this work has succeeded in reducing heat exchanger size, generally there has been little decrease in heat exchanger mass, with a marked penalty in pressure drop across the device. The remaining central question is then: how can the mass and size of tomorrow's compact heat exchangers be decreased while minimizing the increase in pressure drop.

Two general categories of improvements are apparent. In the first, the mass can be reduced directly by replacing the material from which the heat exchanger is constructed with lighter material of similar or improved strength and heat transfer characteristics. The second option centers on the enhancement of the heat transfer mechanism within the heat exchanger. This area of research involves techniques aimed at altering the interaction of the internal heated surface and the passing fluid to increase the heat transfer coefficient at the interface. By doing so, a given thermal load will require a smaller and lighter

heat exchanger. Many options exist for such enhancement, and can be classified in two major categories:

1) Passive - any technique not requiring a direct external energy expenditure
2) Active - any technique requiring the direct input of energy into the system in order to maintain the heat transfer enhancement

The field of heat exchange enhancement is quite diverse. According to Ohadi [14], approximately 20 different heat transfer enhancement techniques across both system types are in use today in a broad range of applications.

One active technique that has shown promise in this regard is electrohydrodynamics, or EHD. In flow systems, EHD deals with the introduction of an electric field into the flow field of a working fluid. In this technique, the high voltage, low current electric field is applied across all or part of a flow channel containing the fluid by use of various types of charged and grounded electrodes. The primary result of this coupling is the generation of secondary flow within the thermal boundary layer, as seen in Figure 1, thus increasing bulk transport away from the heated surface and enhancing the advection portion of convection heat transfer.

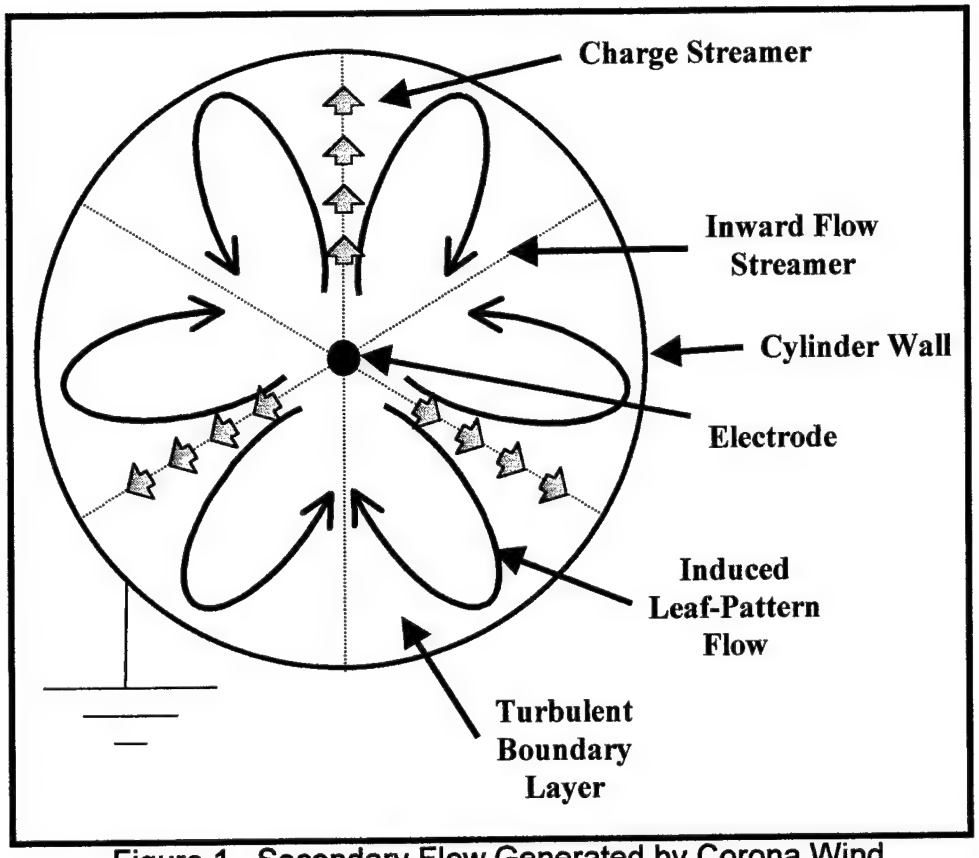

Figure 1. Secondary Flow Generated by Corona Wind

Knowledge of this effect is certainly not new. The ability of an electric field to affect the heat transfer characteristics of a fluid media has been investigated since the 1930's when Senftleben [10] first investigated its effect on gases. Kronig and Ashman [1], in the late 1940's, were the first to work with EHD in liquids. Over a half-century of work in the field has shown that EHD techniques are effective in dramatically increasing convection heat transfer coefficients. The general characteristics of EHD enhancement are [14,5]:

1) Heat transfer enhancement due to EHD is roughly proportional to the strength of the electric field.

2) Up to four fold increases in heat transfer have been observed in single phase systems (20x in two phase).
3) The pressure drop penalty in flow systems has been shown to be low.
4) The energy expenditure required to maintain enhancement is typically minimal with fluids of low electric conductivity.

Of particular interest to the Department of Defense is the potential for EHD to provide an "on-demand" heat transfer enhancement capability within an airborne weapons system. This would allow heat exchangers using EHD technology to be designed to the average expected thermal load instead of the maximum system load currently used to scale airborne heat exchange equipment. The EHD enhancement could be activated only in the more extreme flight or performance regimes, where higher thermal loading would occur. Such a design approach would enhance the overall performance of the weapon system by freeing valuable mass and size for allocation to other subsystems.

1.2. Problem Statement

Given proper research and development, electrohydrodynamics may have potential for widespread application in Air Force systems, including both airborne weapons systems and ground based support systems. The Air Force Research Laboratory (AFRL) is currently a member of an EHD consortium with institutions from academic, commercial, international, and U.S. government sectors. However, most of the recent scientific and commercial effort in EHD

R&D is focused on development of EHD for commercial applications, especially in large industrial and residential HVAC systems. The majority of the research, therefore, has been empirical in nature for the purpose of identifying appropriate fluids and electrode geometries for inclusion in these systems. However, to fully investigate the potential for this technology to fulfill unique Air Force thermal management requirements aboard the next generation of military aircraft, the AFRL desires the ability to perform basic EHD experimentation "in-house".

The problem addressed here, then, is the need for a validated, experimental EHD test facility within AFRL. This study will develop, integrate, and validate a medium scale, closed fluid loop for the investigation of EHD heat transfer enhancement for dielectric fluids in square channel, laminar flow. This study will establish the baseline for the Transparencies and Thermal Systems Branch, Flight Dynamics Directorate, Air Force Research Laboratory for further investigation into EHD applicability for aircraft heat exchanger miniaturization, or HEM. Bulk thermodynamic fluid properties will be used to evaluate loop integration and performance.

1.3. Summary of Current Knowledge

In order to more fully understand what has been accomplished thus far in electrohydrodynamics as it relates to internal flow forced convection heat transfer, a review of applicable literature was conducted. The nature of EHD lends it to be studied in a wide range of regimes. EHD research in the last 50 years has included work on free and forced convection, condensation, pool

boiling, fusion, solidification, and others. The effects of a large number of variables, including electric field nature and strength, electrode geometry, fluid type, flow regime, heat transfer surface geometry, and many others have been studied [10].

The effect of an electric field on the heat transfer characteristics of fluids has been known since the late 1930's. In 1931, Senftleben [10] first reported on the effects of an electric field on the natural convection heat transfer within a gas. This discovery spawned an immediate interest in electroconvective phenomenon. However, it wasn't until 1951 that Ahsmann and Kronig [1] accomplished the first research in electroconvection using liquids as the working fluid. These first experiments used an experimental setup consisting of a short cylindrical tube, which served as the electrode, coupled with an axial, 20 μm platinum wire heater. Even in these initial tests, in which relatively low potential electric fields were introduced into the flow fields of several organic liquids, a 50% increase in heat transfer was realized. They also extended to liquids a Nusselt number correlation found in their earlier gaseous EHD work. These promising first steps in liquids prompted more investigation.

For the next decade, researchers attempted to pinpoint the enhancement mechanism at work in dielectric liquids under EHD. The progression of this work was well covered by T.B. Jones in 1978 [10]. Through the 1950's and 60's, fundamental characteristics of liquid-EHD interaction were uncovered. Weber and Halsey [19] first postulated that the fluid body force due to EHD had three components. Schmidt and Leidenfrost [10] found a minimum threshold for EHD

to be effective. In 1957, Mascarenhas [13] presented his ideas for the existence of two distinct EHD effects dependent upon field strength. He claimed existence of a low field effect, uncoupled from the flow, and later confirmed by Senftleben and Schnabel [10] to be due to an increase in thermal conductivity of the fluid, caused by the electric field. He also presented a high field effect based on electroconvection with a field strength threshold. Many others, including Allen [2] and Care and Swan [10] worked to explain a low field convection inhibition by investigating space charge buildup around electrodes, charge relaxation time dependency, and fluid applicability for EHD heat transfer enhancement.

In 1968, Thornton [10] reported on unpublished experiments by Porter which focused on forced convection EHD enhanced heat transfer. In these experiments, a heated cylinder and axially mounted thin wire electrode were used with an insulating oil working fluid to achieve a 100% increase in heat transfer coefficient, when coupled with a strong dc electric potential (15 kV). This marked one of the first integrated investigations into the effect of a strong electric field on heat transfer and hydrodynamic disruption in forced convection.

Coupling EHD research with heat exchanger technology research began in large part in the late 1970's and continues to this day. The heat exchanger geometry of choice during this period was an annular cylinder. Ohadi [15] reports that these experiments, including those by Poulter, Miller, Fernandez [8], and Levy [12], showed maximum heat transfer coefficient increases up to 2300% using a variety of industrial fluids of low electrical conductivity.

The last decade has seen an increase in basic empirical studies with dielectric flow systems. In 1991, Ohadi et al [15] used air-air, single pass, shell and tube heat exchangers fitted with dual side electrodes to investigate steady state heat transfer enhancement and pressure drop penalty for varying shell and tube flow rates and EHD voltages. This study used heat transfer and pressure drop measurements as well as pump power calculations to evaluate optimal ranges for EHD enhancement of heat transfer. The three phases of the experiment involved using EHD applied to only one side at a time, and then on both shell and tube sides. A maximum enhancement of over 300% was shown to occur when both sets of electrodes were used. Generalized optimal ranges for EHD enhancement were claimed to occur at low to moderate Reynolds numbers within the laminar regime, and at electric potentials in the midrange between the incipience threshold and dielectric strength. Corona current due to increasing corona voltages for constant conditions were also measured for both the shell and tube sides. The optimal ranges for EHD, although only roughly determined, can be beneficial for a zeroth order baseline test scaling for dielectric liquid experimentation.

1.4. Objective and Scope

The primary objective of this study was the development of an electrohydrodynamics test rig at the AFRL. Flow testing of a single dielectric fluid was used to evaluate test section and loop performance and integration. The fluid chosen was Flourinert FC-72, an electronic cooling fluid. The process

for choosing this fluid can be found in Chapter 3. Flow conditions were scaled to the laminar and transition regimes, and the applied voltage for EHD enhancement was limited to direct current. The test section consisted of a single, fixed geometry square channel containing a flat heater element opposed by a high voltage electrode grounded to the heater across the 3 mm fluid gap. Since the test section used in the experiment was not designed with integrated instrumentation, temperature and pressure data were collected at the inlet and exit. While the inlet conditions were maintained constant, changes in the outlet conditions were used to evaluate test section integration, using bulk thermodynamic data reduction.

Since on-demand heat transfer enhancement is a probable Air Force use for EHD, further studies on the loop investigating the transient nature of the phenomenon are expected in order to develop control laws for the mechanism. EHD has been shown to have a larger effect in two-phase fluids than in single phase fluids. With this in mind, the objective of this study was to develop a test loop that, with minor modifications, could be used for both of these extensions.

1.5. Methodology

A fluid loop for use as an electrohydrodynamic experimentation rig was developed and installed in AFRL's Transparency and Thermal Systems Laboratory at Wright Patterson AFB. This loop was designed for testing single-phase fluids in forced convection laminar and transition flow through a test section of small hydraulic diameter. This loop and its validation tests are for use

as a zeroth order baseline for the purpose of guiding future EHD fluid loop and test section modification and development for a wide variety of possible follow-on testing.

A single pass, rectangular-channel test section was installed in the test loop. Since neither the loop nor the test section had been used before, several characterization and validation tests were necessary before data runs could be accomplished. These tests included:

1) Stringent leak checks
2) Development of loop operating procedures, such as process fluid fill
3) Loop temperature settling time characterization
4) Flow generation and measurement validation
5) Thermocouple and transducer validation and calibration

The following tests were run to verify proper integration of the fluid loop, test section, and data acquisition system:

1) Pool fluid extraction test
2) EHD voltage scaling
3) High voltage isolation test
4) Low voltage telemetry sensitivity checks

A more detailed description of these validation procedures can be found in Chapter 3.

Since a bulk thermodynamic analysis of inlet and outlet conditions would be used for data reduction, the differential temperature and pressure across the test section were the most critical measurements. A differential thermocouple measured the mean temperature difference between inlet and outlet flows. Test section differential pressure was measured by installing a differential pressure transducer in parallel with the test section. An absolute pressure transducer was also installed directly upstream of the test section.

Other measurement devices in the experimental setup included a Coriolis mass flow measurement system. This flowmeter provided working fluid absolute temperature, specific gravity, and mass flow rate. A high voltage power supply provided a measurement of the voltage supplied to the EHD electrode and the resulting corona current. The telemetry from the low voltage power supply included the current and voltage supplied to the test section heater strip. Gross visualization of the flow within the test section was provided by a standard video camera.

Three data sets were collected during this experiment: one baseline set with no EHD voltage and two sets with EHD voltage applied. The two sets with EHD voltage on were taken with two heat input levels, while varying EHD voltage. Absolute temperature at the inlet of the test section was maintained at a constant level throughout all tests, and was not used as a test variable in this study.

II. Theory

In order to successfully investigate the heat transfer enhancement in single-phase fluids due to electrohydrodynamics, the theoretical background of the subject should first be understood. In developing a test rig for such research, an understanding of the basic relationships governing the fluid-electric field interaction is no less important. Therefore, an overview of the applicable hydrodynamic and electrical theory is presented here. The focus of this discussion is steady state, forced convection in single phase, incompressible fluids, although some mention of other test regimes may be of benefit to future research, and will therefore be briefly included.

2.1. Hydrodynamics

Since electrohydrodynamics involves the manipulation of a working fluid by use of an electric field, we would expect the effect to manifest itself as an alteration of the typical hydrodynamic governing equations for viscous, incompressible fluids. The popular forms of these equations, as described by Jones [10], Yabe [21], and others, follow.

For conservation of mass within the flow system, the continuity equation takes the form of:

$$\frac{\partial \rho}{\partial t} + \nabla \bullet \left(\rho \bar{u}\right) = 0 \qquad (1)$$

where: ρ = density of the working fluid, kg/m^3

$\bar{u}$ = fluid velocity, m/s

Applying the assumption of steady state flow yields the simple incompressibility condition:

$$\nabla \bullet \bar{u} = 0 \qquad (2)$$

This assumption is reasonable since this study deals primarily with single phase, Newtonian fluids.

Conservation of momentum within the control volume of the inter-electrode space of the test section gives this electrohydrodynamic form of the Navier-Stokes equation:

$$\rho\left(\frac{\partial \bar{u}}{\partial t} + \bar{u} \bullet \nabla \bar{u}\right) = -\nabla p + \mu \nabla^2 \bar{u} + \rho g + f_e \qquad (3)$$

where: ρ = Fluid density, kg/m^3

μ = Fluid dynamic viscosity, kg/(m sec)

g = Gravitational acceleration, m/s^2

f_e = Electric body force density acting on the liquid, N/m^3

Conservation of energy is an important relationship for heat transfer problems involving electrohydrodynamics. The relationship represented here is derived assuming negligible compressional work and viscous dissipation.

$$\frac{\partial T}{\partial t} + \bar{u} \bullet \nabla T = \alpha \nabla^2 T + \frac{\sigma_e E^2}{\rho c_p} \qquad (4)$$

where σ_e is the electrical conductivity of the fluid and $\sigma_e E^2$ represents ohmic heating due to current, generated by the applied electrical field, passing through

the fluid. This term is typically small for applications involving insulating liquid dielectrics.

2.2. Maxwell's Equations

Coupled with these equations are the governing equations for the electrostatics side of the EHD formulation. The reduced Maxwells equations break down into the following, as outlined in Davidson and Kulacki [5], Jones [10], Yabe [21], and others. Poisson's equation defines the free charge density in the dielectric fluid, ρ_c as:

$$\nabla \bullet \varepsilon \overline{E} = \rho_c \tag{5}$$

The conservation of electric current, J, yields a result similar to continuity:

$$\frac{\partial \rho_c}{\partial t} + \nabla \bullet \overline{J} = 0 \tag{6}$$

For a coupling of flow and electric fields, the definition of electric current density changes from the standard form to:

$$\overline{J} = \rho_c \overline{u} + \sigma_e \overline{E} \tag{7}$$

where: ρ_c = Space charge density within the fluid, C/m^3

σ_e = Electrical conductivity of the fluid, $ohm^{-1}\ m^{-1}$

The $\rho_c \overline{u}$ term accounts for the movement of fluid free charge due to the fluid velocity, while the $\sigma_e \overline{E}$ term is the current across the fluid gap in the direction of the electric field lines and dependent upon the electrical conductivity of the fluid,

σ_e. The standard definition of electrical potential is presented here for completeness of the listing.

$$\overline{E} = -\nabla\phi \tag{8}$$

or from the definition of a conservative field, ϕ:

$$\nabla \times \overline{E} = 0 \tag{9}$$

where: ϕ = Electric potential, V

E = Electric field strength, V/m

2.3. EHD Bulk Force Density

The most important portion of the proceeding development is the electric force density term, f_e, found in the incompressible Navier-Stokes equation. This term represents the reaction of the fluid molecules to the applied electric field. The nature and size of this interaction depends upon the electric field's uniformity and field type as well as the dielectric and polarity properties of the fluid. Although the expression of the electric force density term can vary, the most widely accepted form for convective heat transfer systems is [10], [5], [4]:

$$\overline{f}_e = \rho_c\overline{E} - \tfrac{1}{2}\,E^2\nabla\varepsilon + \tfrac{1}{2}\,\nabla\left[E^2\rho\left(\frac{\partial\varepsilon}{\partial\rho}\right)_T\right] \tag{10}$$

where: ρ_c = Fluid space charge density, C/m^3

ε = Dielectric permittivity, F/m

Chang and Watson [4] include terms in the formulation of the force density equation dealing with the effect of a magnetic field on the fluid, only to state that

these terms would be negligible for all except liquid metal systems, resulting in the expression above.

The three terms of the force density equation merit further discussion in order to make clear their significance in different regimes. The first term, $\rho_c \overline{E}$, is defined as the Coulomb force density, and is the force per unit volume acting directly on the free charges in the fluid. The second term represents the force density due to a gradient in the dielectric constant, or electric permittivity, within the working fluid. The third term is defined as electrostriction by most authors, and is due to forces exerted on molecules polarized by a non-uniform electric field.

As seen in the first term, the Coulombic interaction of the flow and electric fields is dependent upon the existence of free charge within the medium. The generation of this free charge is a topic of continuing investigation and modeling [16]. For systems with electrolytic solutions as the working fluid, as is the case in electrokinetics, the fluid is readily ionized. Therefore, the production of ionic species within the fluid is the dominant source for free charge. However, for an insulating dielectric fluid, the mechanism seems to be much different.

Dielectric fluids, by definition, are not readily ionizable. The free charge in these liquids is due to two main sources: simple electric conduction, assumed negligible by most due to the high electrical resistance of the fluid, and gradients in the conductivity and permittivity of the fluid. These gradients are due to a thermal gradient within the fluid and the temperature variability of the electrical parameters [10], [21]. In contrast, the Taylor-Melcher leaky dielectric model, as

covered in depth by Saville [16], attributes the free charge to unipolar injection of ions at the electrode. However, Saville states that the Coulomb force term is still negligible for dielectrics since the fluid-electric field coupling only occurs at the electrode interface, and therefore free charge within the bulk fluid is negligible.

The fluid free charge, and thus the effect of the Coulomb force term, can be increased by the introduction of more conductive material into the dielectric media. This has two disadvantages. First, the conductive material alters the thermodynamic properties of the working fluid. Second, the discharge field strength is reduced dramatically, thus lowering the effect of all terms in the electric force density equation.

Electric permittivity gradients within the fluid media have been shown to produce a force on the bulk fluid. In single-phase fluids, these gradients are due to fluid temperature differences across the electrode gap. Ahsmann and Kronig [1] used the relation

$$\nabla\varepsilon = \left[\frac{\partial\varepsilon}{\partial T}\right]_\rho \nabla T + \left[\frac{\partial\varepsilon}{\partial\rho}\right]_T \nabla\rho \qquad (11)$$

to express the nature of the dielectric permittivity within the media. This statement simply treats the dielectric gradient as a function solely of the fluid thermodynamic state and uncoupled from the electric field.

For two-phase fluids this term can be much more substantial. The large difference in dielectric permittivity between the liquid and gaseous states of a fluid generates a strong dielectric permittivity gradient at the vapor-liquid

interface. This effect has been shown to have a dramatic effect on the nature of the boiling mechanism in two-phase EHD testing.

Uniformity of the electric field is a critical variable in analyzing an EHD system. EHD heat transfer enhancement is driven by the generation of secondary flow within the thermal boundary layer. This flow is due to the reaction of both charged particles and neutral molecules to the local electric field. How these particles react depend heavily upon the uniformity and strength of the field. Figure 2 is taken from Singh [17], and shows the behavior of various particles within a uniform electric field.

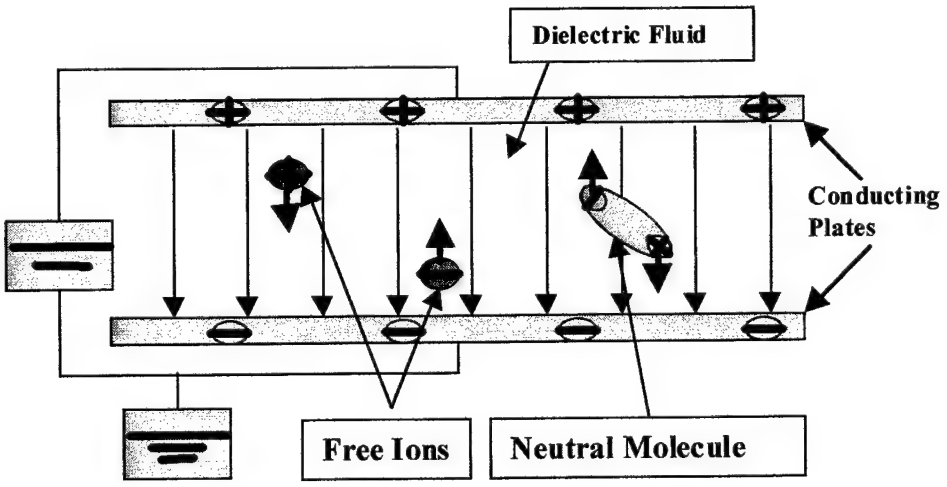

Figure 2. Behavior of Charged and Neutral Molecules in a Uniform Electric Field, Singh [17]

The figure shows a dielectric fluid between two, parallel, flat plate electrodes. If a high voltage is applied across the plates, a uniform electric field is generated

within the dielectric field. The magnitude of this field, assuming a constant dielectric number throughout the fluid, is

$$E = \frac{V}{\kappa d} \tag{12}$$

where: V = Voltage supplied to the electrode, V

κ = Dielectric constant of the fluid

d = Electrode separation, m

Coulombs Law gives the force on each free charged particle or ion as:

$$\overline{F}_p = q_p \overline{E} \tag{13}$$

Thus, each freely charged particle will be acted upon by the electric field, will move along the local electric field lines, and in doing so will interact with other particles, causing a disruption of the thermal boundary layer and increasing the heat transfer rate from the heated surface.

The vast majority of molecules in a high purity dielectric liquid, however, are not ions, but electrically neutral. A neutral molecule in a strong electric field will tend to polarize, or distort along the bonds to create a separation of charge centers within the molecule. The ability of a compound to display this characteristic is a function of the atomic structure of the substance. If the dielectric molecules have appreciable polarizability, α, the molecules of the fluid will rotate to align with the local field. However, since the field is locally uniform, the particle will not translate, and thus will not contribute to the boundary layer disturbance [17].

In a non-uniform electric field, the free charges will act the same as in the uniform electric field, traveling along field lines toward the electrode of opposite polarity. The neutral particles, however, will translate as well as rotate to field-align. Figure 3 graphically displays this mechanism. Although it is electrically neutral, the polar molecule translates due to field strength differential between the charge centers of the molecule. In Figure 3, the electric field, and thus the force on the negative polarity of the molecule is greater than that of the positive side. Singh notes that switching the polarity of the electrodes will not affect the translation of the neutral molecules, since the movement will always be toward the region of higher electric field density.

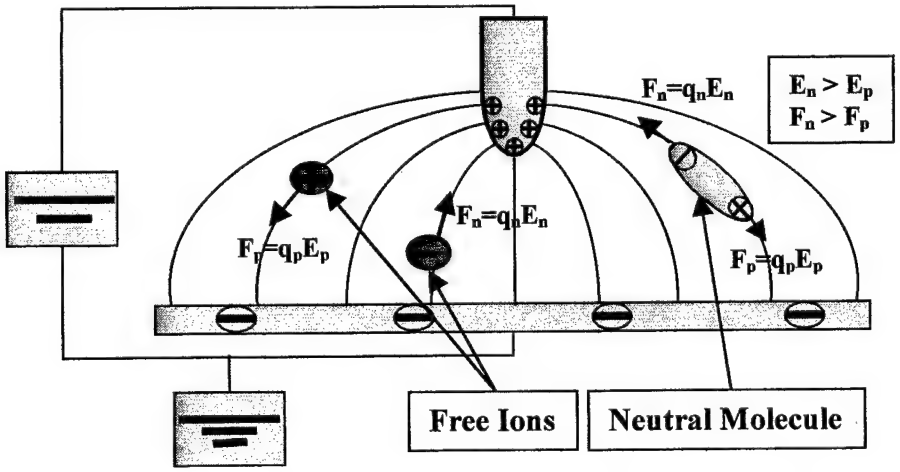

Figure 3. Behavior of Charged and Neutral Molecules in a Nonuniform Electric Field, Singh [17]

As seen in this development, the equations governing electrohydrodynamic enhancement of heat transfer are highly coupled, and therefore have not been solved analytically for complex flow systems. While the EHD relations are of little help in the accurate analysis of convection systems,

they yield important general insight into regimes in which EHD would be most effective. Clearly, a stronger electric field will generate a higher EHD response, as will a highly non-uniform electric field or a large dielectric gradient existing at a phase change boundary. This study will use these general relations to guide the development of an experimental EHD test rig, and to explain the results of validation testing on the loop.

III. Experimental Setup

3.1. Test Loop

The success of an experimental research effort is highly dependent upon the design quality of the experimental apparatus and the test matrix. Since EHD research had not previously been accomplished in this laboratory, the development of an experimental test rig for use there was an iterative process continuously coupled with engineering forethought. Many problems were overcome in the development of this loop. Remaining challenges are outlined in Chapter 5 - Conclusions and Recommendations.

3.1.1. Design Criteria / General Description

The desire of the Air Force Research Laboratory to have fundamental in-house EHD testing capability at minimal cost drove the general design. The test rig used in this research was developed using a moderate list of design criteria. From the outset, the general design goals for the experimental test loop were:

1) Useful for single phase fluid testing with only minor modifications necessary for two-phase fluid testing
2) Compatible for steady state or transient regime heat transfer research
3) Highly integrated with data acquisition system for maximum computer control of telemetry measurement and test variable settings

4) Minimal flow disturbance and pressure effects throughout the loop

5) Minimize potential for hardware corrosion and rust on wetted surfaces

6) Ease of loop assembly and disassembly

7) Simple loop operation

8) Stay within lab project budget by maximizing use of parts currently on hand in lab

The test loop resulting from the above design goals consists of a closed process fluid loop with a removable heat transfer test section. Supplemental components consist of an integrated, Pentium-based data acquisition system, a suite of computer controllable power supplies, a process fluid reservoir, and a cold water chiller loop. These major components are broken down and explained in the following sections. For general reference, Figure 4 is a schematic representation of the entire experimental test setup, and Figure 5 is a picture of the test section end of the process fluid loop.

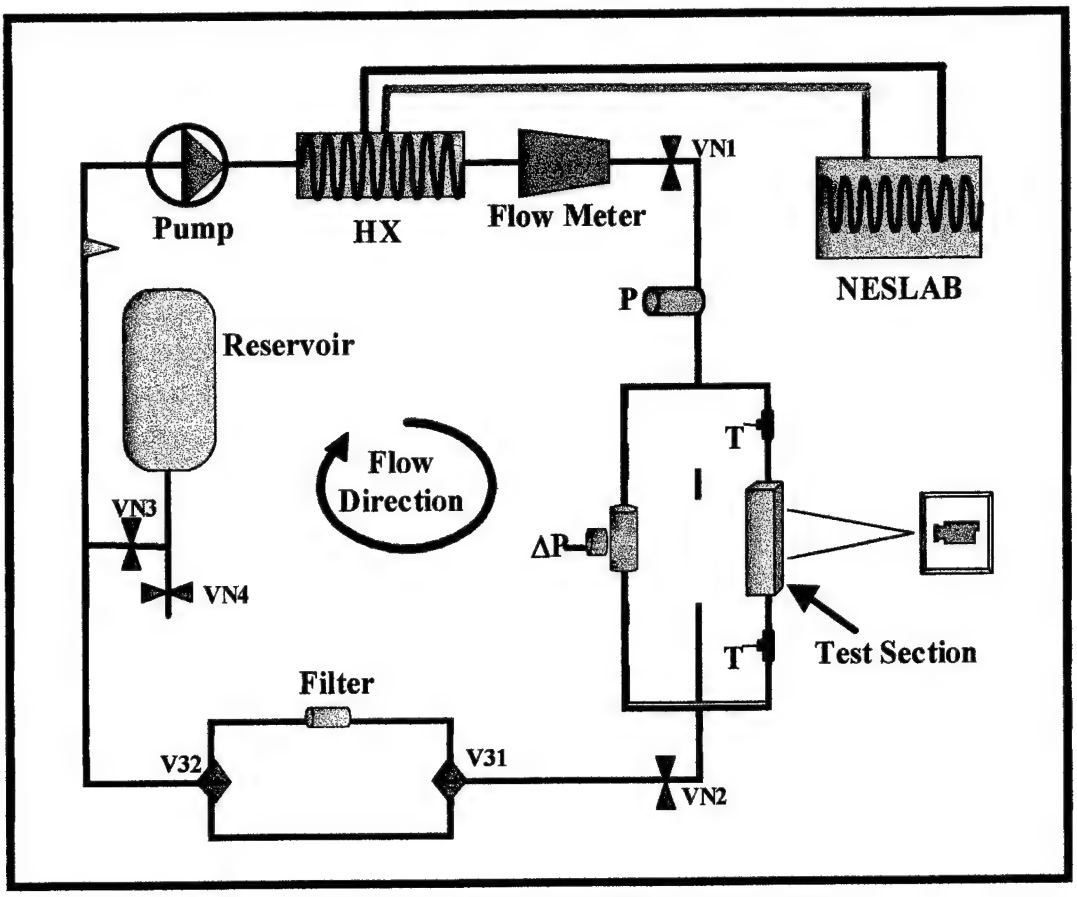

Figure 4. Experimental Test Rig - Schematic

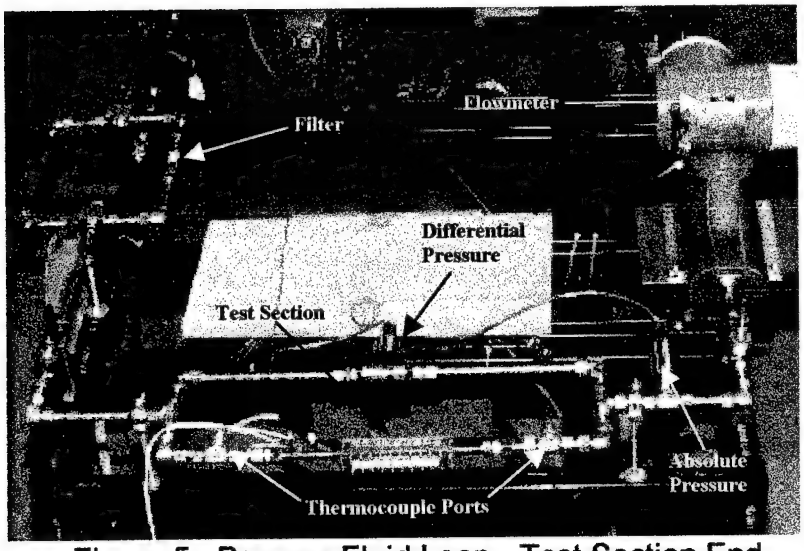

Figure 5. Process Fluid Loop - Test Section End

3.1.2. Fluid Control and Flow Measurement

The purpose of the Fluid Control and Flow Measurement components are to provide controllability and containment of the working fluid, precise measurement of the fluid flow parameters (flow rate, temperature, and density), while resisting corrosion and providing ease of operation. The components contained in this system are:

1) Stainless steel tubing and Swagelok connectors
2) Ball and needle valves
3) Process fluid reservoir tank
4) Magnetic gear pump
5) Coriolis flow meter

The majority of the loop consists of 0.4 inch inner diameter circular stainless steel tubing. The choice of stainless steel was a common one for most wetted loop components, since it is highly resistive to corrosion, rusting, and other adverse reactions with the candidate working fluids. Such interactions between the loop hardware and the process fluid could generate contamination within the loop, a highly undesirable condition discussed later in this chapter.

Since a first generation experimental setup should be expected to withstand much assembly and disassembly, the components and connectors must be durable. In a loop of this nature, the parts most susceptible to assembly damage are the tubing and connectors. Stainless steel tubing of this gauge

provides good durability, and no problems were encountered in this area through numerous loop breakdowns and component changeouts.

The majority of the connections in the loop were made using Swagelok compression fittings. This type of fitting makes loop changeout operations quite easy, and the loop design easily alterable. When possible, major loop components were chosen with this connection standard in mind. Only where loop components were not easily compatible with Swagelok standards were these fittings not used.

Numerous valves were used throughout the setup to isolate loop sections for vacuum leak checks, control filling of the loop, bypass the filter, and isolate the reservoir from the loop. Figure 4 shows the location of the seven valves used in the loop. Four of the valves are needle valves, designated in Figure 4 as VN*x*. The two three-way ball valves, designated V3*x*, were used to bypass the filter. A Schrader valve was installed in the loop between the reservoir branch and the pump for quick connection of vacuum or pressurized air.

A process fluid reservoir was incorporated into the experimental setup to provide a controllable method for fluid introduction into the loop. The reservoir is a stainless steel 5-gallon tank with a 1 inch threaded bottom drain piping, a large oblong, sealable top hatch, and various topside ports, one of which houses an absolute pressure gage. This tank is vacuum capable, and is outside the main process fluid loop, connected by stainless steel tubing and a separation valve from the drain piping. Another needle valve serves to control tank dumping.

More discussion on the operation and use of the reservoir is included in Appendix E.

Establishing steady flow within the loop is critical to generating meaningful heat transfer data, especially in future transient studies. For this loop several types of pumps were considered, including diaphragm-, progressing cavity-, impeller-, peristaltic-, and gear-based pumps. Criteria of steady flow, compatibility with candidate fluids, computer controllability, and cleaning ease were considered and resulted in the incorporation of a magnetically driven gear pump from Cole Parmer Instrument Company. The pump consists of two components, a digital drive controller and a pump head. When connected, magnets within each interact to provide pumping power. This setup has three advantages, isolation of the drive unit from the process fluid, protection of the drive unit from overtorque, and flexibility of use with multiple flow rate pump heads.

The pump driver unit is a Pro-Spense® Digital Drive from Cole Parmer Instrument Company. This unit has a 0-4000 rpm motor speed range with +/- 0.2% speed control via either manual control from the front control panel, or a serial RS-232 protocol direct connection to the data acquisition computer. Currently this connection is used only on the command side.

Two Micropump® gear pump heads were used in this experiment. The low flow rate pump head is rated for 0.092 milliliters per revolution, while the high rate head is rated for 0.94 ml/rev. Using these pump heads with the drive

controller at 7.5% to 90% maximum motor speed (4000 rpm), yields the following flow rate ranges:

Table 1. Pump Head Flow Rate Ranges

Pump Head	Flow Rate (ml/min) Pump Speed:7.5% Max	Flow Rate (ml/min) Pump Speed: 90% Max
Low	27.6	331.2
High	282	3384

The selection of these pump heads allowed for adequate overlap within the flow rate range. The pump speed limits of 7.5% and 90% are used here to avoid regions of probable magnetically decoupling of the pump head from the driver.

Precise measurement of the mass flow rate is required on this test rig, since it is a critical parameter in convective heat transfer experimentation. For this measurement a Coriolis mass flow rate measurement system manufactured by Endress and Hauser is used. The process fluid flows through the Promass 63 in a 1/12 inch inner diameter tube. This tube is subjected to an oscillation at its natural frequency. The resulting Coriolis force within the fluid causes a shift in the tube's oscillation phase. This phase shift is dependent only upon the mass flow rate through the tube. This method of mass flow rate determination is both non-intrusive and accurate, delivering uncertainties of +/- 0.2%. The Promass 63 also provides fluid density and temperature within 0.02 kg/l and 0.5 ^{o}C. The Promass 63 can be controlled directly from the front panel via an

infrared sensed, touchless control panel or through a serial RACKBUS/RS-232 protocol connection with the data acquisition computer.

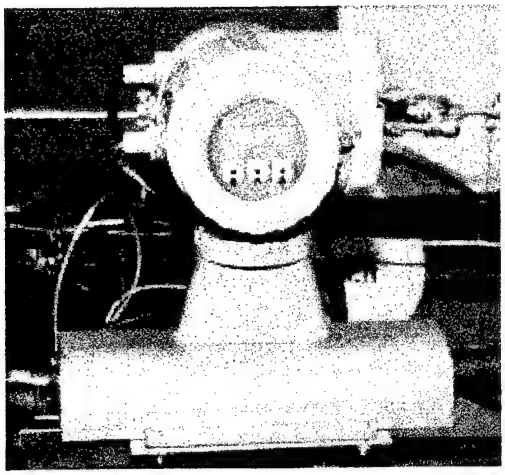

Figure 6. Coriolis Flowmeter

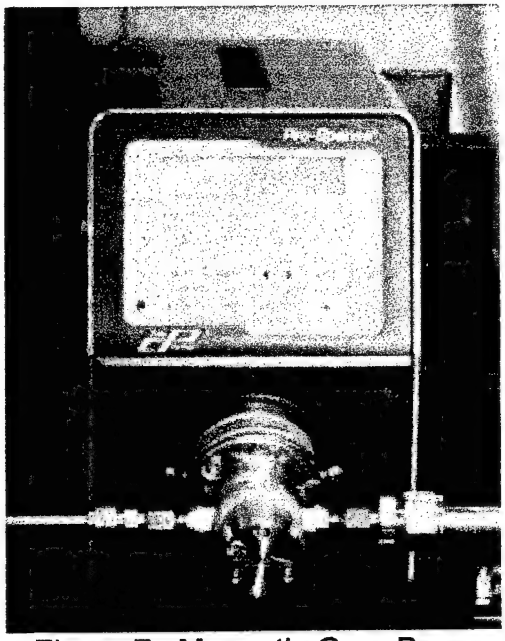

Figure 7. Magnetic Gear Pump

3.1.3. Fluid Temperature Maintenance

Several components in the test rig are included to maintain the temperature of the process fluid throughout the duration of the test. These components are:

1) Process fluid heat exchanger
2) NESLAB Chiller
3) Tube Insulative Wrapping

In our testing, heat is input to the process fluid by a resistive heater strip in the test section. Since the rig is a closed loop system, this energy input must be counteracted or the fluid temperature at the input of the test section will vary over the course of the test. Such variation is not acceptable for high accuracy heat transfer testing. An inline heat exchanger is therefore required to maintain the fluid temperature at a constant, commanded level.

Several heat exchanger designs were considered for inclusion in the loop, with primary criteria of fluid compatibility, rust and corrosion resistance, and small pressure drop on the process fluid side. Initially, a large shell and tube heat exchanger was chosen and installed in the loop. This heat exchanger, along with some reservoir fittings, highlighted for the first time the importance of loop cleanliness, to be discussed in detail later, as they contained components prone to rusting.

The search for a new heat exchanger with no oxidizable wetted parts resulted in the selection of the one pictured in Figure 8. This small heat exchanger was originally designed for use as an oil cooler on an airborne platform. Since it was designed for extended term use, both the single pass oil side and the dual pass fuel side were constructed of stainless steel. Component validation testing data showed minimal pressure drops on both sides at 25% higher Reynolds numbers than this experiment expected to observe. The heat transfer capacity was calculated from validation data provided with the unit, and was found to be approximately 5000 W, far greater than needed with this test loop.

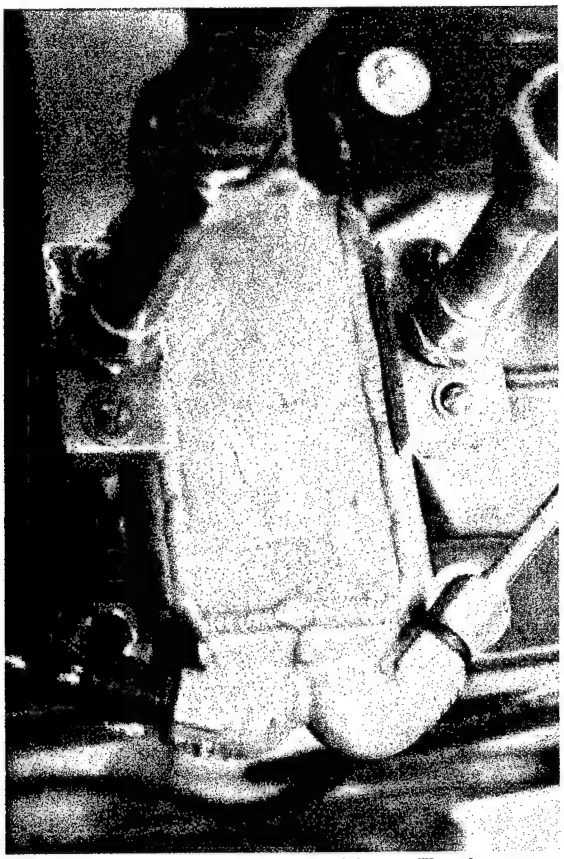

Figure 8. Process Fluid Heat Exchanger

This heat exchanger was installed in the loop with the dual pass side serving the process fluid, and a constant temperature water source connected to the single pass side. The chiller used for cooling the heat exchanger is a NESLAB cold water chiller system. This unit is rated for 10,000 W, and can be set for an outlet temperature range of 3 to 30 °C. Externally insulated copper piping is used for the cold water loop. To further eliminate process fluid temperature variation at the test section inlet, all plumbing between the heat exchanger and the test section was wrapped in cylindrical foam pipe insulation.

3.1.4. High and Low Voltage Support

The test rig requires several types of electric service. Most components, such as the pump, flowmeter, and data acquisition computers require standard 120 VAC service. However, four power supplies are required to provide special electrical support to other components of the test rig. The test section is designed for two types of electrical support, high voltage direct current service for the EHD electric field, and low voltage direct current service for the internal resistive heater. In addition, each pressure transducer requires a steady 10 VDC input.

Two Hewlett-Packard 6033A low voltage power supplies are used to provide the required 10 VDC excitation voltage to the differential and absolute pressure transducers. One Hewlett-Packard 6033A low voltage power supply generates the specified power to the test section heater strip. These three power supplies are identical and are controlled from and monitored by the data acquisition system via an IEEE 488 daisy chain. They are capable of providing 0 to 20 V and 0 to 30 amps.

A single Glassman high voltage power supply (HVPS) generates the strong EHD electric field within the test section. This unit is capable of supplying voltages from 0 to 40,000 VDC and current from 0 to 50 milliamps. The HVPS voltage and current is commanded remotely by two 0 to 10 VDC signals from a digital to analog converter on the IEEE 488 daisy chain. Output voltage and current telemetry from the HVPS are 0 to 10 VDC supplied to the data acquisition input board. The HVPS is connected to the test section through a

shielded high voltage supply cable. The test section end of the cable was fitted with a standard automotive sparkplug female connection, with a large insulative rubber boot. This boot provides good corona containment by covering the entire sparkplug post on the test section.

3.1.5. Temperature and Pressure Measurement

3.1.5.1. Differential Thermocouple

Precise temperature measurement near the test section is critical to the generation of quality heat transfer data. Since the test section in this study, as discussed in Section 3.4, was not designed for heat transfer testing, external data collection was required. Comparison of the bulk thermodynamic properties of the inlet and outlet flows required accurate measurement of the differential temperature across the test section. Two methods for this could be used with the available E-type thermocouples from Omega. The most obvious solution is taking measurements from two separate thermocouples, one mounted at each end of the test section. However, this approach results in the derived differential temperature containing roughly double the uncertainty of a single thermocouple. By using one instrument to measure differential temperature directly, the uncertainty of a single thermocouple can be achieved. Thus, a differential thermocouple was designed and constructed from two standard E-type thermocouples. The design used in this experiment is derived from the fundamentals of thermocouple theory.

In 1821, Thomas Seebeck discovered that if two dissimilar metal wires are connected at both ends, forming a loop, and one junction is heated, current would flow around the produced thermoelectric circuit [18]. Figure 9, taken from the Omega temperature handbook shows this. If the circuit is broken across both metals, the resulting Seebeck voltages are a function of the respective junction temperature. However, if the circuit is only broken in one location, as seen in Figure 9, the resulting voltage will be the difference between the Seebeck voltages of each junction, corresponding to a difference in temperature between the junctions.

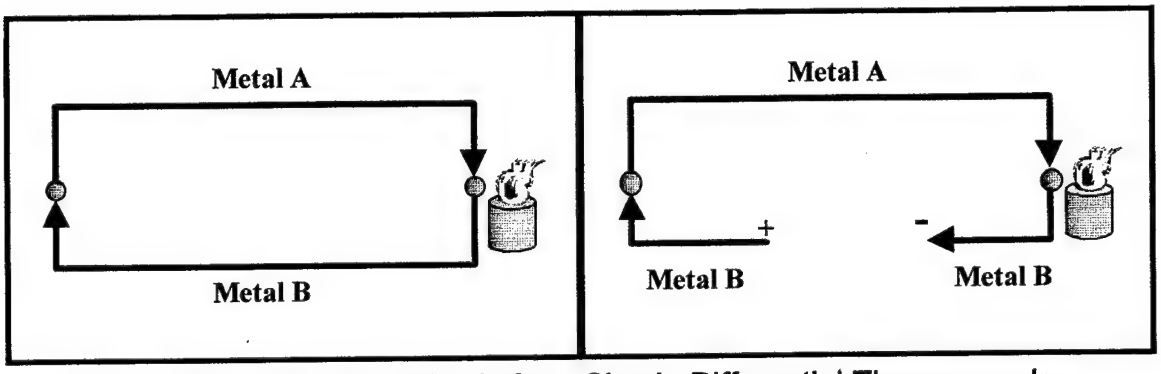

Figure 9. Theoretical Basis for a Simple Differential Thermocouple

The differential thermocouple constructed for this study was derived from two identical E-type thermocouples. These thermocouples contained a 1/16" diameter, unshielded, ungrounded junction of Nickel-Chromium (Ni-Cr) and Copper Nickel (Cu-Ni). As shown in Figure 10, the two negative poles of the thermocouples were connected together with copper nickel thermocouple wire, while nickel-chromium wire was used to connect the positive sides to the data acquisition board.

Any dissimilar metal junction along a thermocouple loop, such as connecting to a data acquisition board, can cause an additional, unwanted Seebeck effect. The configuration of the differential thermocouple effectively nullifies such an error since both connections to the acquisition board are the same dissimilar metal junction. Assuming the acquisition board connections remain at the same temperature, the Seebeck voltages will act in opposite directions and effectively cancel. Therefore the voltage measured from the differential thermocouple is due strictly to the difference in temperature between the Ni-Cr / Cu-Ni junctions within the thermocouple probe tips.

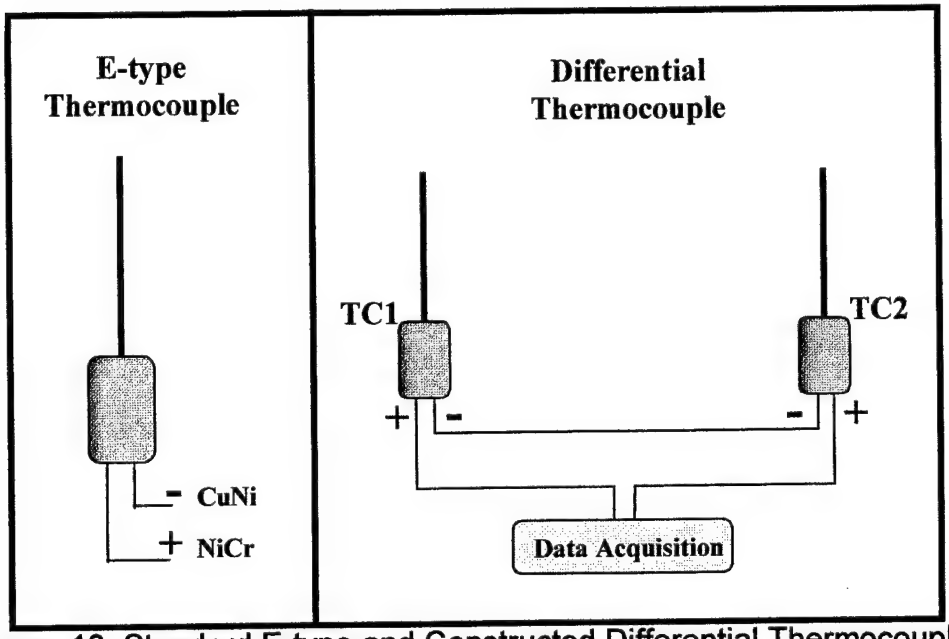

Figure 10 Standard E-type and Constructed Differential Thermocouples

The newly constructed differential thermocouple was calibrated using a constant 0 °C reference point on one thermocouple while subjecting the other to slowly varying temperatures. Figure 11 shows the setup used for this calibration.

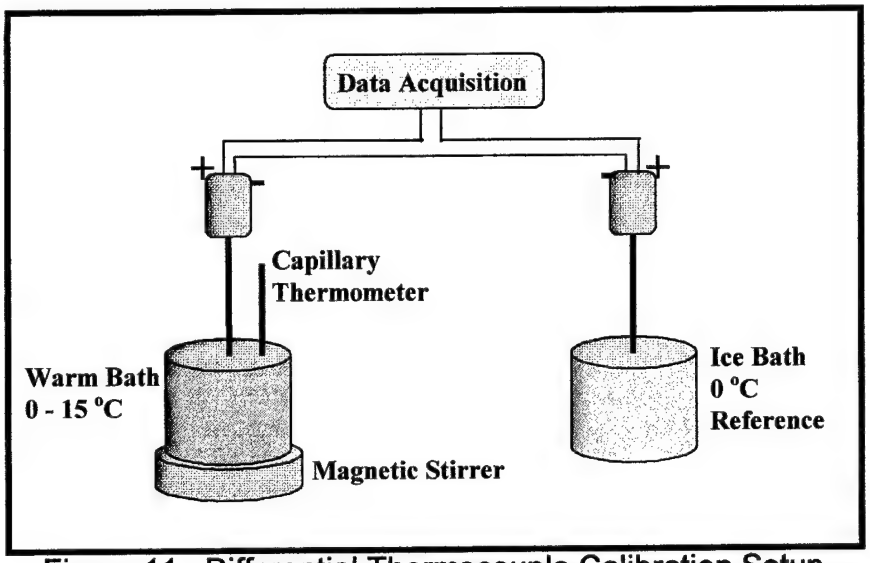

Figure 11. Differential Thermocouple Calibration Setup

The warm bath was started as a 0 °C ice slurry and allowed to warm up slowly at a rate of approximately 10 °C per hour as monitored by a capillary thermometer with accuracy of +/- 0.05 °C. A standard laboratory magnetic stirrer ensured a near homogeneous temperature was maintained throughout the bath during the calibration. Data was taken every 0.5 °C from 0 to 15 °C for the positive temperature differential (TC1 warmer than TC2). The calibration was repeated from 0 to 4 °C in 0.5 °C increments with the thermocouples switched to achieve better calibration accuracy near the 0 °C differential temperature point. Data for a true 0 °C differential temperature was taken by placing both

thermocouples in the 0 °C reference point. The resulting calibration curve was highly linear. Calibration data can be found in Appendix B.

3.1.5.2. Absolute and Differential Pressure Transducers

Electrohydrodynamic forces acting on a fluid passing through a closed vessel have been shown to increase the pressure drop across the vessel. This effect is an important consideration for future use of EHD within flow systems, and is therefore a standard test measurement in EHD experimentation. In the development of this test rig, two types of pressure measurement were incorporated.

As can be seen in Figure 4, the test section portion of the process fluid loop is branched, one side containing the test section and thermocouples, and the other side containing a differential pressure transducer. The size of this branched section was minimized in order for the differential pressure transducer to observe the same pressure drop as across the test section.

The differential pressure transducer used for this measurement was the industrial Sensotec HL-Z, containing a bonded foil strain gage in a double jacket stainless steel casing. It is capable of measuring differential pressures of 0 to 50 psid with an accuracy of +/-0.25% of full scale.

Measurement of the absolute fluid pressure was also desired for use in data presentation and for future parametric studies. Therefore, a Sensotec Super TJE absolute pressure transducer was installed between the flowmeter and the upstream junction of the test section branch. This Super TJE is

designed for absolute pressures between 0 to 50 psia, and is accurate to within +/- 0.05% of full scale. This transducer also uses a bonded foil strain gage and a double jacket stainless steel casing.

As mentioned in the electrical power section, both transducers require a 10 VDC excitation voltage, resulting in telemetry output of approximately 20 mVDC at full-scale conditions of 50 psid/psia. Both transducers were calibrated in-house using the setup shown in Figure 12. The setup for the differential pressure transducer calibration was identical to the one in Figure 12, except a gage pressure head was used to measure the differential from atmospheric pressure, while the negative end of the differential pressure transducer was left open to atmosphere.

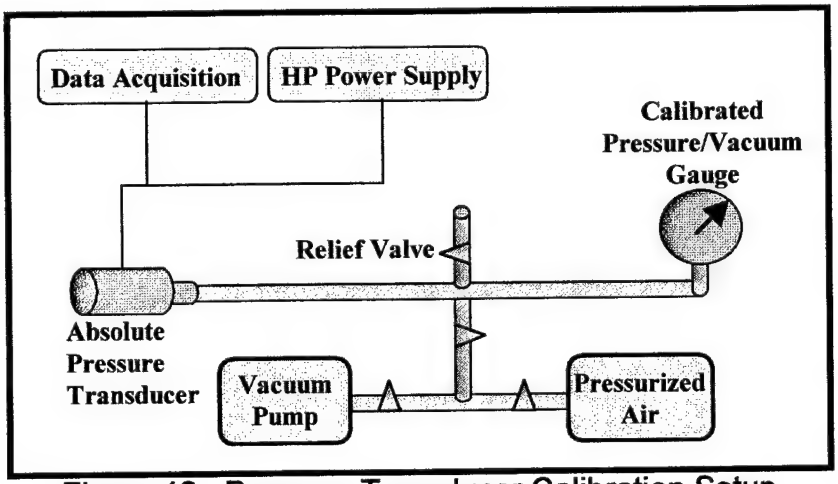

Figure 12. Pressure Transducer Calibration Setup

Data for the differential pressure calibration were taken across the entire range of the device, 0 to 50 psid in 5 psid increments. To improve the calibration resolution around 0 psid, several data points were taken at a slightly

negative differential pressure. The absolute pressure calibration varied pressure from approximately 1 psia (lower limit of the vacuum pump) to the upper range of 50 psia in 5 psia increments. Both calibrations were done twice, once in each direction, with identical stop pressures. Assuming that strain gage and pressure head hysteresis changed linearly during the calibration, using the average of the two data points for each pressure effectively minimized this effect. The calibration curve for each device was found to be highly linear. Calibration data can be found in Appendix B.

3.2. Contamination Control

There are two strong reasons for fluid contamination control to be a concern in the development of an EHD test rig. First and most obvious is that contamination of the process fluid would alter the heat transfer characteristics of the working fluid, thereby skewing the data generated from such an experiment. Secondly, hardware and electrostatic field interactions with contaminated fluid can adversely affect the operation and safety of the loop.

The introduction of contamination of any form into the process fluid will change the electrophysical properties of the fluid mixture. As explained in Chapter 2, electrohydrodynamic enhancement of heat transfer within a dielectric working fluid requires a strong electrostatic field. Coupling this requirement with heat exchanger design goals of minimal power consumption and slow or non-existent fluid breakdown leaves a desired operational regime where the electrostatic field does not generate sparking within the fluid. The probable

outcome of a contamination event is reduction of the maximum field strength before electrostatic discharge, hereafter called the sparkover voltage. Depending on the geometry of the test section and the nature of the contaminant, this reduction of the sparkover voltage can be due either to a lower electrical resistance within the fluid or to the build up of residue along a vessel wall. Either one will allow discharge at lower field strengths than for a pure dielectric fluid and clean test section.

Aside from reduced heat transfer benefit, such sparkover, especially for long duration, can have adverse effects on the hardware and fluid involved. Process fluid acting as a pathway for discharge can be chemically altered due to the high energy density of the discharge. 3M, manufacturers of the FC-72 used in this experiment, reports that at around 250-300 ^{o}C, FC-72 undergoes thermal decomposition into hydrogen fluoride and perfluoroisobutylene, both deemed hazardous in trace amounts by OSHA. Also, experience from this research effort revealed that sparking within the test section increased wall residue along the discharge path, further lowering the sparkover voltage. Finally, electrostatic discharge within the proximity of sensitive data acquisition or heat generation components places expensive hardware at risk of damage.

To control contamination in this test rig, a high-grade disposable filter unit manufactured by Balston was used. The filter is constructed of borosilicate glass with a fluorocarbon resin binder, and is rated 98% retention efficiency for 0.3 μm particulate. To ensure filter compatibility with the process fluids, an

agitation bath was used. After three hours in high agitation, no discernible breakdown of the filter was observed in FC-72 or ethylene glycol.

3.3. Data Acquisition System

The data acquisition and loop control systems were designed to enable the user to have maximum control over data gathering and loop parameter control. The goal in this study with respect to the data acquisition system was to support its in-lab development, validation, and integration with the test rig. The extended-term goal for this data acquisition system is an automated test control and data acquisition capability.

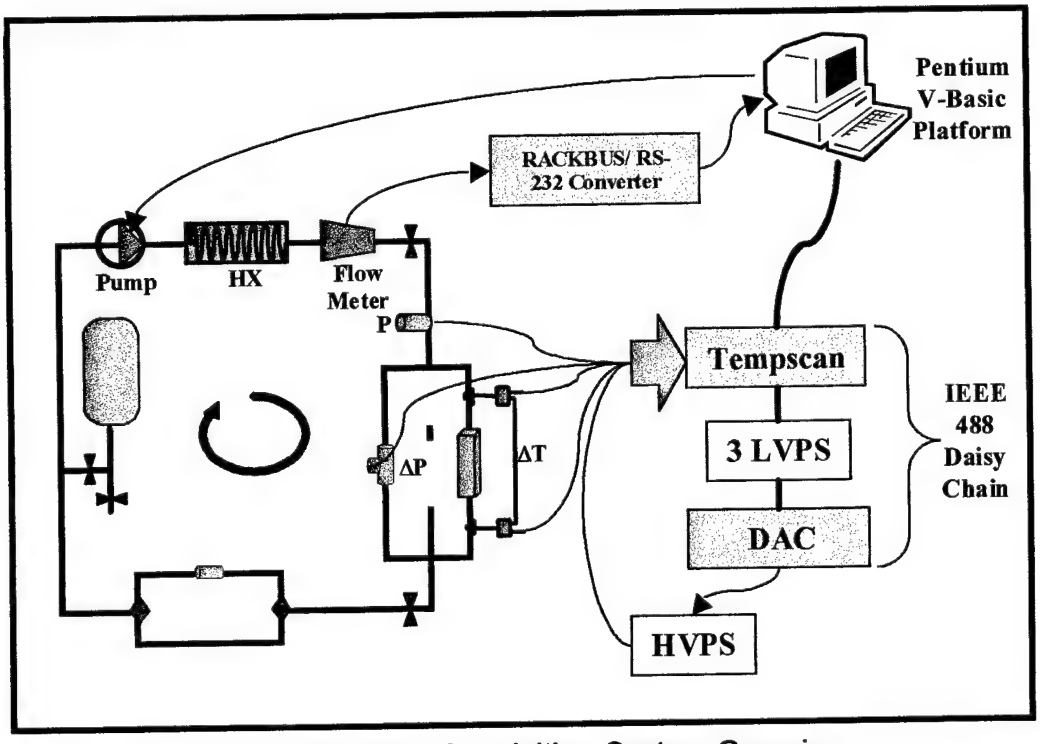

Figure 13. Data Acquisition System Overview

Figure 13 is an integrated overview of the data acquisition system and the developed experimental test rig. The core of the system is a Pentium-based personal computer manufactured by Micron. A graphical user interface (GUI) developed in Visual Basic provides a front-end environment for data acquisition control. This V-basic routine, developed in-lab, allows convenient control of pump speed, high and low voltage power supplies, and input of user observed variables for inclusion in the generated data file. Routines for sensor calibration, test variable observation, and data acquisition are easily initiated from the GUI environment.

Control and measurement of the low and high voltage power supplies and the temperature and pressure measurement devices in the loop is accomplished through the use of an IEEE 488 daisy chain connecting the PC, low voltage supplies, and a set of IOtech data acquisition equipment. The IOtech suite consists of a Tempscan/1100 high speed voltage measurement unit and a DAC 488/HR-4 digital-to-analog converter.

The Tempscan/1100 with a TempV/32B voltage scanning module contains 32 input channels with programmable ranges of +/-100mV, 1V, 5V, and 10V. It is capable of scanning at 960 channels per second with 16 bit resolution. It is designed for 10V channel to channel isolation, and 500V channel to system isolation. This device is used to measure five channels of loop telemetry. Three channels are set to the 100mV range and sense the voltages produced by the differential thermocouple and the two pressure transducers. Two channels are

set to the 10V range and sense the current and voltage telemetry from the HVPS.

The digital-to-analog converter is used for control of the HVPS. As mentioned earlier in this chapter, the HVPS output voltage and current is commanded using individual 0 to 10 VDC signals corresponding the 0 - 20 mA and 0 - 40,000 V ranges of the device.

3.4. Test Section

The most critical portion of the test rig is the heat transfer test section. This section of the loop is where the process fluid interacts with a locally applied electrostatic field and a separate heat source.

This test section was originally designed for EHD effect presentation and visualization. Figure 14 shows a schematic of the test section. This test section simulates parallel plate channel flow heat transfer by establishing a constant geometry channel bounded by materials of high thermal resistance. This channel is 72.0 mm long, 2.9 mm wide, and 3.2 mm tall, for a hydraulic diameter of 3.0 mm. The channel is bounded on the top and bottom by two macor (ceramic) insulative platforms mounted on a thin stainless steel channel body. The ceramic inserts are separated by the 3.2 mm gap width, and provide large thermal and electrical resistance. Thin film silver plating on the entire gap surface of each ceramic insert serves as the resistive heater and EHD electrode.

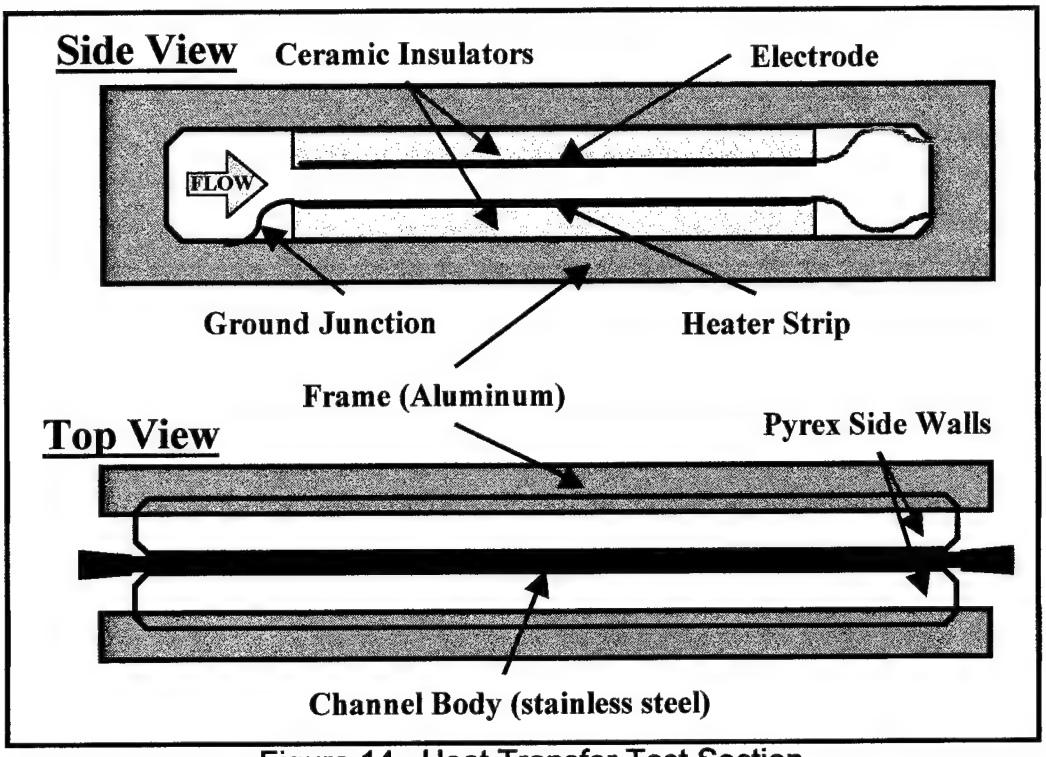

Figure 14. Heat Transfer Test Section

The walls of the heat transfer channel are made of 1/2 inch Pyrex glass. The use of Pyrex allows for visual observation of the EHD effect while maintaining a non-reactive, thermally insulative environment around the channel. A thin Teflon sheet is inserted between the channel body and ceramic and the Pyrex glass for better flat surface sealing. The aluminum frame of the unit comes in two pieces, machined for coupling with the Pyrex glass, and fastened together by 24 bolts.

The inlet and outlet ends of the test section body have been tapered and welded to 0.4 inch stainless steel tubing, allowing for easy connection to standard Swagelok fittings. A five hole manifold was included within the tapered

section, with two outlet holes and one inlet hole used for routing heater, electrode, and ground wires.

The silver strip electrode on the upper ceramic insert generates the near-uniform electrostatic field within the test section. The heater in the test section is a simple resistive heater made of silver plating applied to the lower ceramic insert. Both silver strips are approximately 2.9 mm by 72 mm, with the heater having a measured resistance of approximately 0.2 ohms. Current for the heater is supplied from one low voltage supply to an insulated nut and bolt connection on the outlet body tube. The electrode is energized through a high voltage spark plug connection on the outlet tube. Both supply wires are routed through the outlet manifold and to the downstream end of the respective ceramic inserts.

The stainless steel body of the test section serves as the electrical ground for the device. A ground bolt for the test section is located near the heater supply connection, and should always be connected to an external ground when power is supplied to either the heater or electrode. The heater is grounded to the body by a welded connection on the upstream end of the heat transfer channel. The electrode is grounded across the fluid gap and through the heater strip to the same ground weld.

3.5. Loop Validation Tests

Once the loop components were selected, individually validated, and installed in the test rig, a series of integration testing was required to verify that

the test rig as a whole performed as expected. This section outlines the most significant of these tests.

3.5.1. Fluid Choice / Pool Fluid Extraction

A number of fluids were presented as candidates for this single phase, EHD fluid experimentation. The limited capability of the lab to handle hazardous material confined the choices considerably. The fluids considered for this study were:

1) Deionized water: for use as a baseline fluid only
2) Ethylene glycol: a standard industrial coolant
3) Poly-alpha-olefin (PAO): a dielectric synthetic coolant
4) Flourinert FC-72: a dielectric electronics coolant

This list of candidate fluids was reduced further by a simple test similar to dielectric strength testing. This test makes use of the Liquid Extraction phenomenon, described by Yabe [21] and Singh [17] as the instability of a dielectric gas-liquid interface under an EHD environment. In this phenomenon, a charged electrode brought in close proximity to a dielectric liquid surface causes the liquid to extend through the gas toward the electrode. With a high enough potential, an extracted liquid "bridge" will close the gap. While this phenomenon mostly shows the effect of a strong non-uniform electric field on the phase boundary of a dielectric, it can offer some insight into the dielectric nature

and EHD mobility of the fluid. This simple test also allowed for first-hand familiarization with the EHD phenomena and its effect on a variety of fluids.

The general setup can be seen in Figure 15. Approximately 10 mm of each fluid was placed in an eight inch diameter conductive pan. A high voltage probe was suspended above the middle of the pan, creating an air gap of approximately 3 mm between the probe and the fluid surface. The conductive pan was grounded. The voltage supplied to the probe was slowly increased as the voltage and current was carefully monitored and recorded. The activity of the fluid was also carefully monitored for surface deformation, bridge formation, and gap flow turbulence.

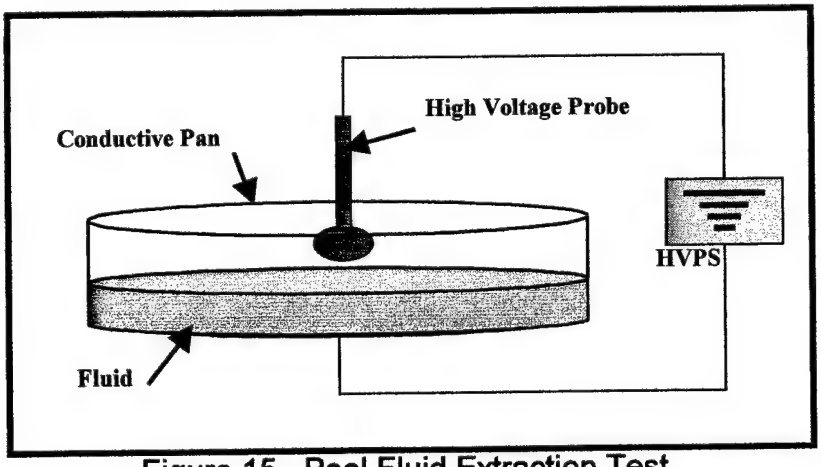

Figure 15. Pool Fluid Extraction Test

The results of this testing showed a marked difference between the fluids. As shown in Table 2, the ethylene glycol was affected by the electrostatic field generated by the probe at a relatively low field strength. Surface deformation was first observed at approximately 1800 V. More importantly, however, was the behavior of the fluid while the bridge was formed, allowing contact between the

electrode and the fluid. Ethylene glycol is not a strong dielectric, and therefore allowed substantial current flow (16 mA) upon fluid bridge formation. Discharge in the gap occurred at approximately 5500 V, very low for any substantial EHD effect to occur.

Table 2. Results of Pool Fluid Extraction Test

	EtGly		FC-72		PAO	
Event	Voltage (V)	Current (mA)	Voltage (V)	Current (mA)	Voltage (V)	Current (mA)
Deformation	1800	0	3100	0	4200	0
Gap Bridged	2500	16	7800	0	6500	0
Max Voltage	5500 *	50	26000	0	23000	0

For the dielectric liquids, FC-72 and PAO, the results of this test were much different. Surface deformation and bridge formation occurred at higher voltages than with the glycol, due probably to the field deadening properties of dielectric materials. More importantly, during gap closure by the bridge, no measurable current was observed. Even as the strength of the electric field was increased and the fluid bridge became increasingly turbulent, negligible current through the fluid was observed. Furthermore, no gap discharge was observed in the dielectric tests. The maximum voltage point corresponded to corona discharge within the probe suspension setup and not through the fluid.

This series of tests demonstrated the strength of the EHD effect on a two-phase boundary. It also highlighted the fact that strong dielectrics are a good fluid choice for systems where low power consumption is a requirement. In general, this series of tests rendered better practical understanding of the EHD phenomenon and its dependence on working fluid. As a result, candidate

working fluids for this study were reduced to only FC-72 and PAO, with FC-72 ultimately used as the sole fluid in this study.

3.5.2. Leak Checks

Before fluid was introduced into the loop, the containment capability of the installed hardware was checked. Since the process fluid side of the test rig is a closed loop system, even an extremely small leak would, in time, result in a substantial amount of air entering the loop. Also, containment and proper disposal of the process fluids is required by Department of Defense HAZMAT regulations. Making the loop leak free is especially important when using fluids such as FC-72, which has a low surface tension.

A helium detector was used in verifying a leak free installation of the loop. This device contained an integrated vacuum pump, and was connected to the Schrader valve located between the reservoir branch and the pump. A helium source with a low flow rate wand was used to introduce helium to the external surfaces of loop connectors, valves, and the test section. Connections requiring tightening were easily identified by a quick increase in the level of detected helium. This method proved successful as no leaks or increase in air within the loop were observed after a successful leak check.

3.5.3. Loop Temperature Settling Time

One concern in using a closed process fluid loop is the possibility that the test section inlet conditions will be difficult to control due to physical feedback mechanisms within the loop. The greatest concern on this loop was the test section inlet temperature settling time following a test variable change. Other similar EHD test rigs within the EHD consortium have exhibited settling times of several hours. Such a long duration between test points would greatly extend the data collection phase.

Using the stainless steel heat exchanger described in Section 3.1.3 alleviated this concern. By using the 5000 watt heat exchanger, which far exceeds the expected energy input from the test section, the loop settling times were virtually instantaneous. Several runs were accomplished to determine the effect on test section inlet temperature, with no change in temperature observed. In fact, throughout all testing, the steadiest measurement was flow meter temperature. The use of an overdesigned heat exchange system alleviated this concern.

3.5.4. EHD Sparkover Voltage

Perhaps the most critical variable in this study is the strength of the electrostatic field. EHD experimentation in the 1950s [13, 2] showed that a threshold voltage must be exceeded for a direct current electric field to affect a liquid dielectric. Other studies by Ohadi [15] and many others show a strong dependence of heat transfer enhancement on electric field strength. It is

therefore important for the upper limit of the EHD voltage to be as high as possible in our testing. However, the upper limit in testing must not exceed the discharge voltage for that set of flow conditions. As mentioned previously in Section 3.2 and covered in more detail in the next chapter, routine electrical discharge within the test section is highly undesirable. The EHD voltage limit must therefore be carefully scaled for the test section and for each process fluid.

Upper limit checks were accomplished during FC-72 flow through the test section. The operating premise of these checks was that discharge would occur at lower EHD potentials for lower fluid flow rates. This is due to increased fluid residence time within the channel allowing for more complete polarization of the working fluid. The checks were therefore run at 5% maximum pump speed. High voltage power supply current and voltage were observed and recorded by the data acquisition system as the EHD voltage was slowly increased from 0 to 25,000 VDC. No internal discharge, EHD current, or effect on the working fluid was observed throughout the entire test range. The maximum EHD voltage for data runs was therefore set at 25,000 VDC. Close visual observation of the test section during testing above 20,000 VDC ensured that any early sparkover due to low level contamination would not be sustained.

3.5.5. Low Voltage Telemetry Sensitivity Checks

Experimental EHD research is challenging for many reasons. One of the most challenging issues is the use of high potential electric fields in close proximity to low voltage-measuring equipment. Isolation from electrical

disturbance is always an issue when attempting to sense low voltage telemetry from thermocouples or transducers, but becomes especially difficult in an EHD environment. Electrical interference can manifest itself in many ways. On this test rig, the following paths were of major concern:

1) Loop charging
2) EHD field induction
3) Process fluid charge transport
4) Ground loop interference
5) Power supply coupling

To ensure isolation of the low voltage telemetry from loop power and signal sources, a series of sensitivity checks were run. The test section body acts as the heater and electrode ground. Since the test section is connected to the loop through stainless steel compression fittings, the potential exists for heater or electrode power to charge the loop, even though the test section is earth grounded through a grounding nut on the outlet tubing. To mitigate this possibility, loop tubing and connections were checked from the flowmeter to the filter branch at slowly increasing heater and electrode power settings. A small charge was noticed on the thermocouple housing. However, since the original thermocouples were grounded, the thermocouple channel displayed a large error traced to the low power heater, but not the high voltage EHD electrode.

A two-fold solution was implemented. First, additional braided grounding cable was connected to the inlet and outlet tubes of the test section to

encourage charge containment within the test section. Second, the grounded E-type thermocouples used to construct the differential thermocouple were replaced with ungrounded, exposed junction thermocouples. The same differential design was maintained, and the new differential thermocouple was recalibrated using the same method as outlined in Section 3.1.5.1. However, the use of the unshielded thermocouple increased concern over charge transported by the fluid affecting the temperature measurement. The exposed thermocouple junction in the process fluid downstream of the test section would be more susceptible to free charge injected by the electrode. As discussed in Chapter 2, the amount of free charge present within a dielectric liquid is a topic of varied opinion among the experts in the field. Although most developments neglect the bulk free change in dielectrics, the effect of the field on the thermocouple through any path would need to be determined.

To determine the effect of this and other electrical pathways on the accuracy of the thermocouples and transducers, an oscilloscope was connected to the thermocouple as the heater and electrostatic field powers were varied. The transducers were monitored through the data acquisition system for disturbances. During this session, process fluid flow was set at 70% pump power in order to minimize charge relaxation within the fluid and maximize the potential effect on the thermocouples. This test also served to measure EHD field interference from the high voltage supply cable and electrode.

The results showed adequate isolation of all devices from both high and low voltage systems. Variation on the sensitive thermocouple circuit was within the range observed during calibration.

IV. Results and Discussion

Experimentation in electrohydrodynamic enhancement of convection heat transfer is, by its nature, a challenging endeavor. Exploration of this phenomenon in the laboratory requires elements and theory from fluid mechanics, thermodynamics, electromagnetism, and chemical engineering. Challenges associated with each field were fully encountered in this study. Many of these obstacles were overcome, while others remain to be solved in future developmental testing.

This study amassed a sizable database of practical knowledge and experience in working with EHD. This information and guidance is the main benefit of this study to future EHD researchers, especially those developing test apparatus for experimentation in this field. The majority of this section will be devoted to presenting a practical evaluation of the developed test rig and recommendations for improvements to its design and operation.

4.1. Test Rig Anomalies, Troubleshooting, and Resolutions

4.1.1. Data Acquisition System

Validation and integration of the data acquisition system is a major challenge in the development of an EHD test rig. Sensing low voltage instrument telemetry in connection with a thermally and electrically robust environment such as EHD is inherently difficult. However, the data acquisition

system, especially the IOtech data acquisition hardware, introduced a host of additional problems into the effort.

The IOtech hardware was chosen based on advertised ability to accurately measure multiple voltage input ranges at high channel scan rates. However, problems with the setup became evident during initial attempts at data collection. The absolute pressure transducer (P1A) read approximately 3 psia high while sensing atmospheric pressure. Initial troubleshooting discovered that P1A telemetry corrected itself when the differential pressure transducer (P2D) was disconnected from the acquisition system. It was obvious that the pressure transducers were interacting through some unknown electrical path.

Troubleshooting narrowed the problem to the Tempscan/1100 processing functions. The unit could not maintain isolation between multiple channels. In order to maintain the testing timeline, the following workaround was implemented. Since the signal offset from the transducers due to crosstalk seemed to be constant when all internal and external connections were maintained, relatively reliable data could be expected if all the following conditions were met:

1) All connections are maintained during calibration and testing
2) All channels remain active within the data acquisition hardware
3) Differential thermocouple and transducer sensitivity is negligible during full scale deflection of all other data acquisition inputs

4) Strict configuration is maintained during thermocouple and pressure transducer calibrations, with the same configuration used during testing.

A series of channel isolation tests were performed to evaluate the validity of the workaround. Channel inputs were varied to full scale while all other channels were monitored for crosstalk. The only observed interaction was between the 10 VDC telemetry of the HVPS and the three low voltage channels of the thermocouple and pressure transducers. Therefore the HVPS signals were cut from the telemetry package and the HVPS data read manually from the unit, causing a loss of automated high voltage telemetry, and decreased control of the test rig. While this solution is certainly not optimal, it provided adequate operability for this set of tests. However, this workaround solution limits the flexibility of the system by requiring each sensor to be recalibrated after any change to a data acquisition component. The unknown nature of the isolation problem introduces uncertainty in the performance and accuracy of the system.

4.1.2. Flow Generation and Measurement

As stated early in Chapter 2, steady generation and accurate measurement of process fluid flow is critical to generating meaningful data from an EHD test loop. Unfortunately, during test runs, this test rig experienced problems in one or both of these areas. The Coriolis flowmeter varied widely in

its measurement of mass flow rate, while density and temperature measurements were consistent. This instability has three possible causes:

1) Gas-liquid two phase flow through flowmeter
2) Pump surging
3) Flowmeter operability problem

Two phase flow at the flowmeter location in the loop is unlikely. The heat exchanger is located immediately upstream of the flowmeter, providing FC-72 directly to the flowmeter at 11°C, well below the 59°C boiling point. No appreciable expansion is located immediately upstream of the flowmeter. Moreover, any incidental two phase flow within the loop should be low quality, not containing enough vapor to effect the flowmeter as dramatically as observed in testing.

During early development of the loop, the pump was run through several water flow trials. Although not truly pulseless, the low volume gear space within the pump heads and relatively high motor speed resulted in an adequately steady flow in the test section as observed during filling and testing. Although unlikely, this pump could cause small variations in the flow at the flowmeter. This possibility should be investigated in future work with this loop hardware.

The most probable cause of the flowmeter variance is the last listed option. The flowmeter may have been operating in a limited flow rate mode during the testing. Although an internal variable, which sets the upper range of the expected flow rate, was altered during testing to accommodate the actual

mass flow rate, the condition was still observed. This may have been due to a flowmeter programming and telemetry subtlety not noticed during the testing phase. The solution to this probable cause is increased familiarity with the flowmeter. A greater level of flowmeter validation should result in a more appropriate telemetry protocol for this application and the flowmeter providing high accuracy mass flow rate measurements.

The resulting uncertainty in mass flow rate measurement necessitated alternate methods for its estimation. From flow meter telemetry, $\dot{m}$ was seen to average 4.7 g/sec with a range of +/-1.7 g/sec. A rough, zero bypass pumping speed correlation yielded an $\dot{m}$ of 21.4 g/sec. The thermodynamic analysis using Figure 16, covered later in this chapter, generated an $\dot{m}$ estimate of 4.8 g/sec. This final method was deemed most reliable and was used for calculation of the Reynolds number. These methods of mass flow rate estimation are not acceptable for high accuracy testing, and should be replaced by a validated flowmeter. These calculations can be found in Appendix D.

4.1.3. Contamination Control

Maintaining loop cleanliness was an unforeseen challenge at the outset of this study. While the use of some type of in-line fluid filter seemed prudent, the critical nature of this concern was not appreciated. However, need for strict contamination control became obvious after two electrical discharges, both requiring test section refurbishment, were linked to particulate and water contamination of the loop and fluid.

The need for stringent loop cleanliness was a lesson learned the hard way in this study. After premature electrical discharge within the test section during preliminary EHD Sparkover Voltage testing, the loop was thoroughly inspected. Several components were identified as containing rust-producing materials. This incompatibility and insufficient internal drying after water flow trials coupled to result in the deposit of contaminate residue on all internal loop surfaces. This rusty residue within the test section was determined to be the cause of the discharge, by supplying a low resistance electrical path between the electrode and ground. The components were changed out with rust resistant ones, mostly stainless steel, and water flow testing was banned from the loop, but not before unexpected sustained internal arcing damaged the test section. The loop was fully dismantled and individual pieces were thoroughly cleaned and allowed to air-dry completely before reassembly. Approximately 30 man-hours were required for this procedure.

The necessity for maintaining high fluid purity was also demonstrated during pre-data runs. After simple flow tests, FC-72 was drained from the loop into a large container for later use. The container contained less than one teaspoon of water, not noticed until after the loop purge. Since FC-72 is more than 1.7 times as dense as water, the water was easily extracted from the container. No remaining evidence of water in the FC-72 or container was visible. The FC-72 was reused, resulting in test section sparkover at 5,000 VDC, much lower than the expected 25,000 to 30,000 VDC. The trace levels of water remaining in the FC-72 caused this significant reduction in sparkover voltage, a

strong demonstration of the sensitivity of EHD to dielectric fluid purity. This sparkover effectively destroyed the silver heater strip by causing it to open circuit.

The three data sets were run with no contamination events. Sets B and C were accomplished up to the planned 25,000 VDC EHD voltage without sparkover. However, during breakdown of some loop components after testing was concluded, large grain-sized, silicate-type contamination was discovered in the reservoir and other loop parts. The fact that the sediment consisted mainly of large grains explains the lack of effect on the EHD sparkover voltage. The size of the grains probably prevented the sediment from being transported by the passing fluid. However, the presence of the contamination points to a remaining problem in the contamination control of the loop. Possible sources of the sediment are pressure dislodgment of heat exchanger residue, remaining fluid-material incompatibilities, and bulk fluid contamination.

4.1.4. Test Section

Throughout the course of testing, several modifications to the test section were required. These resulted in less than optimal performance from the test section, but were necessary for continuing development and validation of the loop.

During the first round of EHD Sparkover Threshold testing, the interior of the Pyrex glass became marked with residue during contamination catalyzed discharge within the test section. This required the Pyrex to be removed and

cleaned. Unfortunately, the Pyrex sidewalls, held in place by 24 bolts in the section frame, proved highly sensitive to stress buildup during reassembly. Even under very gradual and methodical tightening of the bolts in an inside-out pattern, the Pyrex began cracking at the inlet and outlet ends. The damage to the Pyrex was extensive enough that further assembly and disassembly using Pyrex was abandoned. The Pyrex was therefore replaced with machined pieces of 7/16 inch thick Plexiglas, after a sample subjected to a 24 hour agitation in a FC-72 bath displayed no visible adverse effects.

The other major modification of the test section was the replacement of the silver heater strip with a 1/100" diameter Nickel-Chromium wire. The silver strip heater was destroyed by an inadvertent discharge during the pre-data test runs. The thin silver film was easily stripped, and the Nichrome wire was stretched across the heater ceramic insert, with the ends wrapped tightly around the heater supply and ground wires. Nichrome wire was chosen due to its availability, ease of installation, and thermally constant electrical properties. The installed Nichrome strip supplied an order of magnitude increase in resistance, from approximately 0.2 ohms for the silver strip to 1.6 ohms for the Nichrome.

The test section used in this study was designed mainly as a high pressure flow and EHD effect visualization specimen, and not for use in the development of an operational EHD test rig. As such, the test section was not designed and constructed with integrated instrumentation in mind. This limits the ability of the user to generate quality heat transfer data by forcing critical

sensors such as high accuracy thermocouples and pressure transducers outside the area of highest interest, the heat transfer channel. This was understood at the onset of the study, and validation testing consisting of a bulk analysis of the thermodynamic properties at the inlet and outlet of the test section was deemed acceptable for this first development step.

Throughout the development of the test rig, the weaknesses of the test section design became clear. The most significant improvement to the EHD test rig became obvious - a redesigned test section. Instead of listing all the shortcomings of the current test section, a description of suggested design goals for an improved EHD specimen is included in Chapter 5.

4.2. Data Set Description

The validation test matrix was limited in scope to include three data sets evaluating the effects of electric field strength and heat input levels on differential temperature and absolute and differential pressures for the laminar flow regime of a single dielectric fluid, FC-72. The three data sets are outlined in the table below. Parameters held constant throughout all sets were flow rate and test section input temperature. Pump power was held constant at 20% with the high rate pump head, resulting in a calculated turbulent Reynolds number of 1950 (see calculations in Appendix D). Inlet temperature, as measured from the flowmeter, was maintained at 11°C +/- 0.2 °C.

Table 3. Description of Modified Data Sets

Set	Description	Resulting Relations
A	*Baseline* - Heater input varied from 0 to 15 W - No EHD voltage applied	ΔT, P, ΔP vs. Q_{in}
B	*Low heat input* - Constant heat input of 1.6 W - EHD voltage varied from 0 to 25 kV	ΔT, P, ΔP vs. V_{EHD}
C	*High heat input* - Constant heat input of 16 W - EHD voltage varied from 0 to 25 kV	ΔT, P, ΔP vs. V_{EHD}
FC-72 testing only		

In set C, the increased heat input to the test section resulted in a low rate phase change at the heater wire surface. Small bubbles were visible travelling into the exit tube, and a vapor space appeared in the upper portion of the downstream mixing section of the test section. Thus, set C data represents a low quality two-phase EHD environment.

Following this series of tests, a fourth data set was attempted using higher heat input and lower flow rate to increase the differential temperature and encourage increased EHD effect. Approximately 30 W input was selected during this test run, with 7.5% pump speed. At the end of set C testing, slight thermally induced bending of the Nichrome wire was observed during a quick increase in heater input power. The resistance of the heater wire was measured and verified to be unchanged. Minimal heater power was applied and increased

slowly. However, even at the gradual rate, the wire expanded a significant distance across the heater-electrode gap at approximately the 20 W level. The heater had been effectively destroyed for higher power testing during the previous test run.

4.3. Data Reduction

This series of tests allowed for validation of the basic functionality of the test rig. Due to the design of the test section, no meaningful EHD heat transfer data could be gathered, as seen by the application of thermodynamic principles, Newton's law of cooling, and the following assumptions:

- Adiabatic test section
- Fully developed flow within the heat transfer channel
- Constant heat flux across the heater wire
- Constant heater wire resistance
- All heat from the heater is absorbed by FC-72
- Steady state conditions reached between data points.

Using the above, the following relation can be derived:

$$q_{in} = q_{conv} = \dot{m} c_p (T_{out} - T_{in}) = hA(T_s - T_m) \qquad (14)$$

where: q_{in} = Heat input from heater, W

q_{conv} = Heat convected from heater surface, W

$\dot{m}$ = Mass flow rate, kg/sec

c_p = Fluid specific heat, J/kgK

h = Convective heat transfer coefficient, W/m^2K

$(T_{out} - T_{in})$ = Difference in outlet and inlet mean temp, K

$(T_s - T_m)$ = Heater surface temperature gradient, K

For constant heat input, mass flow rate, and fluid properties, Equation 14 shows that an increase in differential temperature infers other processes are at work on the passing fluid, such as fluid resistive heating from the electric field or heat input from the atmosphere through a non-adiabatic test section. Using the same assumed conditions, if h were to increase as a result of the applied electric field, the temperature of the heater surface, T_s, would simply decrease, with no effect on ΔT. Thus, any change in the surface heat transfer conditions is undetectable with this test section. Additional heat transfer surface condition measurements are required for useful evaluation of EHD heat transfer enhancement phenomena.

The data generated in the three sets are presented below. A summary of the expected error and discussion of trends in the data follows the data presentation.

Set A

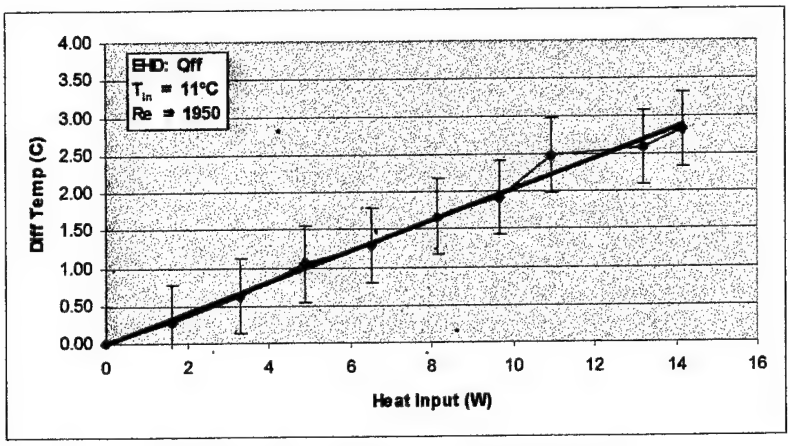

Figure 16. Heat Input Validation

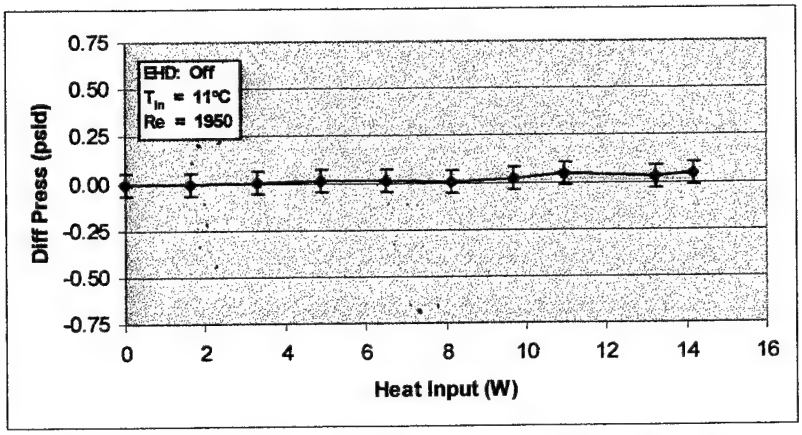

Figure 17. Differential Pressure vs. Heat Input

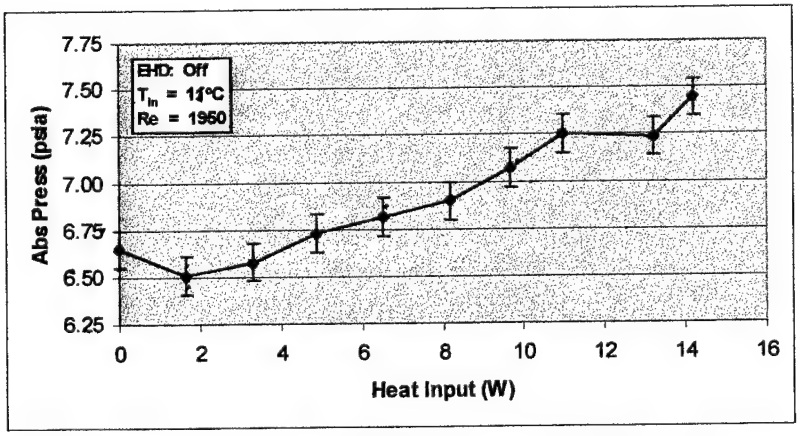

Figure 18. Absolute Pressure vs. Heat Input

EHD Sets B and C

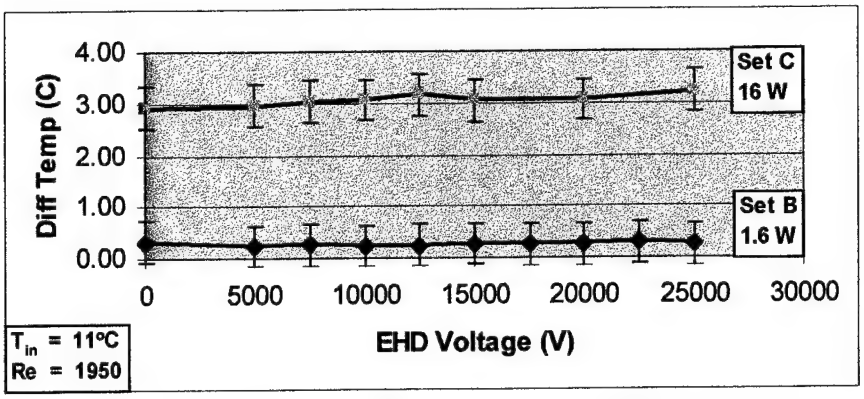

Figure 19. Differential Temperature vs. EHD Voltage

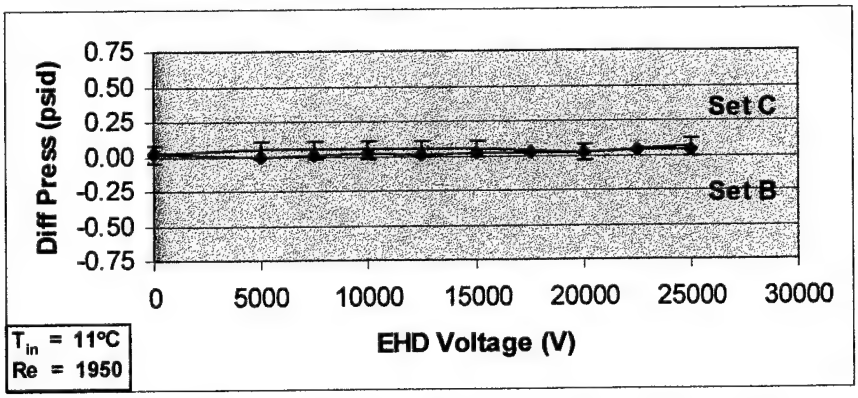

Figure 20. Differential Pressure vs. EHD Voltage

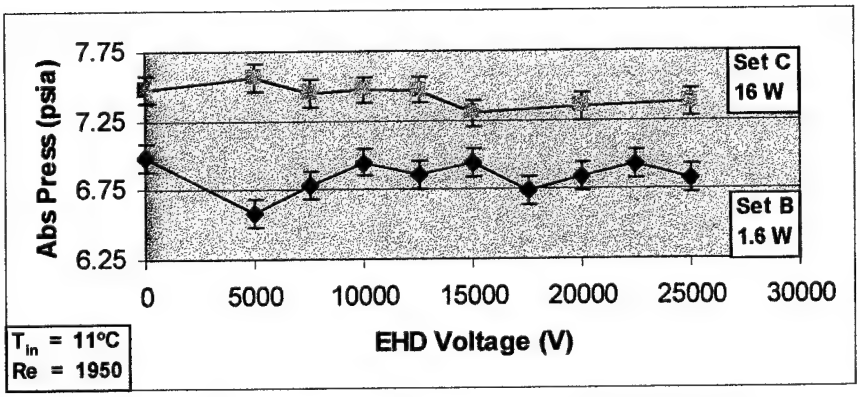

Figure 21. Absolute Pressure vs. EHD Voltage

A summary of the error analysis is presented here to qualify the graphs above before discussing the results. Error sources considered in this error analysis include:

1) Published calibration equipment accuracy (0°C reference, pressure gage)
2) Calibration curve fit error (at the relative range of the measurements)
3) Measurement error

Measurements from the calibrated instruments on this test rig (thermocouple and transducers) are typically considered to approximate a Gaussian distribution [6]. Therefore the accuracy of a data point can be adequately described by a probability that the measurement lies within 'n' standard deviations, or $n\sigma$, from the mean value. For this analysis, a 2σ standard was used, resulting in a 95% certainty that the measurements lie within the error ranges listed in Table 4.

Table 4. Error Analysis Summary

Measurement	Set	Approx. Meas. Range	Error Range (+/-)	Trend Validity
ΔT (°C)	A	3.00	0.52	Y
	B	0.06	0.36	N
	C	0.35	0.40	N
P1A (psia)	A	1.00	0.09	Y
	B	0.40	0.09	Y
	C	0.25	0.10	N
P2D (psid)	A	0.05	0.06	N
	B	0.04	0.06	N
	C	0.04	0.06	N

According to this 2σ analysis, most of the data generated from the testing was within the noise floor of the sensors. As seen in Table 4, the exceptions are set A ΔT and P1A, and set B P1A. However, some observations on test rig and fluid performance can still be made from this data.

Set A differential temperature graph (Figure 16) shows a strong linear relationship between the heater power and the test section temperature differential. This linearity suggests that the test procedures allowed sufficient time between data points for steady state temperatures to be reached. The slope of this graph also helps in the determination of the mass flow rate. As discussed previously, the mass flowmeter was not operating correctly during the test runs, providing wildly varying readings for mass flow rate. Since the slope of the graph approximates $\frac{dq_{in}}{d(\Delta T)}$, and assuming the fluid specific heat, c_p, is known accurately, $\dot{m}$ can be found from:

$$\dot{m} = \frac{1}{c_p} \cdot \frac{dq_{in}}{d(\Delta T)} \qquad (15)$$

Flow rate and Reynolds number calculations can be found in Appendix D.

Sets B and C offered little variation in telemetry readings. This shows that test section differential temperature and pressure and test rig absolute pressure had no dependency on applied EHD voltage. This result leads to two conclusions. The fact that ΔT did not increase in the presence of a strong electrostatic field shows that resistive heating of the FC-72 was negligible in the tested regime. Also, the negligible variation in both the pressure transducers

and thermocouples show that these sensors were sufficiently isolated from the strong electric field.

V. Conclusions and Recommendations

The objective of this study was to develop and validate an electrohydrodynamic experimentation rig for the Air Force Research Laboratory for future fundamental research in EHD enhancement of convection heat transfer. The underlying objective of any first development effort is to substantially increase the practical and operational understanding of the testing process for the subject phenomenon. During the course of this study, a significant amount of groundwork was laid, and should enable further advancement of Air Force Research Laboratory EHD experimental capability in the near future. Recommendations for improvement of several major loop systems are outlined below.

Data Acquisition System

The IOtech hardware used as the core of the data acquisition system simply did not deliver the advertised capability in this application. The marginal workaround, outlined in detail in Chapter 4, was used for this set of testing due to time and budget constraints. However, such a workaround is not an optimal solution for any future work requiring high accuracy low voltage measurement.

Following are several recommendations for improving the data acquisition functionality of the test rig. Foremost, the IOtech hardware, namely the Tempscan acquisition unit should be run through a series of controlled, targeted bench tests to further define the nature of the isolation problem. The results of

these tests will determine whether IOtech equipment has the ability to meet the instrumentation needs of this test rig and the laboratory. In order to build a robust EHD experimentation facility, the data acquisition system must be capable of simple reconfiguration, high accuracy, and high reliability.

Another improvement in the data acquisition system involves modification of the low voltage signals from the thermocouple and pressure transducers. Signal conditioning and amplification would improve the resolution of the data, decrease the susceptibility of the telemetry to system and environmental noise, and relieve the high performance requirement from the data acquisition hardware.

Contamination Control

The success of future testing will depend on the laboratory's ability to control contamination in the loop. Currently, an unknown source of contamination exists within the setup, resulting in the particulate mentioned earlier in the chapter. The source of the sediment should be identified before testing is resumed with the loop. The following is a list of recommendations for cleaning the loop and improving contamination control equipment and procedures:

1) Evaluate all wetted components for extended period material compatibility with all process fluids in an electrostatic environment.
2) Evaluate all new hardware wetted components for the same compatibility.

3) Disassemble the loop and thoroughly clean and dry all surfaces wetted by process fluids.
4) Flush the heat exchanger with a compatible solvent at high pressure.
5) Inspect and filter all bulk process fluids before introducing them into the loop.
6) Improve in-loop filtering method; include a dryer cycle to remove water.
7) Study the long-term effects of EHD on dielectric fluids.

Following a stringent contamination control program, as outlined above, should improve the purity of the working fluid and cleanliness of the loop, thereby reducing the chance of adversely effecting the data or loop hardware.

Test Section

The most critical improvement to EHD testing at AFRL is the design, fabrication, and integration of a new test section into the existing loop. The following set of goals outlines the attributes that a newly designed test section should contain:

1) Minimize flow disruption through the test section by a smooth transition from the loop tubing to the heat transfer channel.
2) Construct the test section body of thermally and electrically insulative material.
3) Design the electrode to produce a non-uniform electric field for a more dramatic EHD effect.

4) Ensure the electrode-to-ground path through the fluid gap is substantially shorter than any other (i.e. along inner wall or to heater).
5) Isolate the heater and the electrode circuitry.
6) Electrically insulate the test section from the rest of the loop.
7) Integrate instrumentation into the test section design.
8) Ensure all wetted parts are fully compatible with all candidate working fluids and cleaning agents.
9) Design for ease of assembly and disassembly with a simple sealing mechanism.
10) Provide a strong, non-fragile design resistant to damage from repeated assembly and disassembly

Using the above goals to design a new test section should greatly increase the validity the testing on this loop. However, integration of all goals mentioned above is a challenging design problem.

Electrode design is key topic in the development of EHD, and has been investigated by members of the consortium. An increased understanding of this subject is needed for efficient test section design.

Instrumenting the test section with flush mounted or sub-surface thermocouples to measure heat transfer channel wall temperature will result in much improved heat transfer data. However, providing electrical isolation of power sources within the test section (electrode and heater) from integrated instrumentation and the rest of the loop is challenging. Possible solutions include using electrically insulative but thermally conductive material to attach

thermocouples to the test section, and plastic flexible tubing for test section connection to the loop tubing. These examples, among others, will give local instrumentation lower sensitivity to and more protection from the EHD electrical environment. Whatever design is implemented, a series of sensitivity checks is necessary to verify negligible interaction between the electrode and heater power and the instrumentation.

Several important areas of knowledge were expanded in this study. The developed test rig generated initial data showing successful basic integration and operation of the test loop, data acquisition system, and support equipment. The Air Force Research Laboratory now has a first generation EHD test loop and a working understanding of the basics of effective EHD test section design, contamination control procedures, and loop design and operation. Deficiencies in several loop components were highlighted and solutions for a more accurate and robust test rig were delivered. Also, identification of a critical flaw in a data acquisition system used throughout the laboratory was discovered, preventing future work on this and other projects from subtle data corruption.

Building on the practical knowledge accumulated during this study, quality heat transfer data should be available from a modified version of this test loop within three months. In order to achieve this, a new test section should be designed, a new data acquisition system integrated into the rig, and a more stringent contamination control program implemented. The test rig validation

should then be a relatively smooth process, resulting in a fully operational, first generation EHD experimentation facility at the Air Force Research Laboratory.

Once the validated rig is online, possible extensions of the research on the rig are numerous. Steady state heat transfer experiments in both single and two phase fluids would serve to increase the size of the subject database, while maintaining the focus on Air Force heat exchanger enhancement. Testing to investigate the transient regime for the EHD effect would aid greatly in the development of useful control laws critical for on-demand heat transfer enhancement. The exploration of various test section and electrode designs would increase the understanding of the practical application of EHD. Fluid parametric studies and long duration EHD exposure tests would contribute significantly to the identification of appropriate working fluids for use with EHD.

It is evident that great potential exists for widespread use of electrohydrodynamics in enhancing the capability of heat exchange hardware. Such an advancement in thermal control technology would contribute to the overall capability of many defense and support systems. This study provides a vital first step for the Air Force in that direction.

APPENDIX A

Error Analysis

Appendix A - Error Analysis

Differential Temperature (ΔT)

Calibration - Error Source	**1 σ**	**2 σ**
Ice Point (0°C reference)	+/- 0.10 °C	+/- 0.10 °C
Calibration Curve	+/- 0.07 °C	+/- 0.14 °C
Total Calibration Error	**+/- 0.17 °C**	**+/- 0.24 °C**
Measurement Error	**1 σ**	**2 σ**
Set A	+/- 0.14 °C	+/- 0.28 °C
Set B	+/- 0.06 °C	+/- 0.12 °C
Set C	+/- 0.08 °C	+/- 0.15 °C
Total Error	**1 σ**	**2 σ**
Set A	+/- 0.31 °C	+/- 0.52 °C
Set B	+/- 0.23 °C	+/- 0.36 °C
Set C	+/- 0.25 °C	+/- 0.39 °C

Differential Pressure (ΔP)

Calibration - Error Source	1 σ	2 σ
Calibrated Pressure Gages	+/- 0.01 psid	+/- 0.01 psid
Ambient Pressure	+/- 0.005 psid	+/- 0.005 psid
Calibration Curve	+/- 0.02 psid	+/- 0.04 psid
Total Calibration Error	+/- 0.035 psid	+/- 0.055 psid
Measurement Error	**1 σ**	**2 σ**
Set A	+/- 0.001 psid	+/- 0.002 psid
Set B	+/- 0.001 psid	+/- 0.001 psid
Set C	+/- 0.001 psid	+/- 0.002 psid
Total Error	**1 σ**	**2 σ**
Set A	+/- 0.036 psid	+/- 0.057 psid
Set B	+/- 0.036 psid	+/- 0.056 psid
Set C	+/- 0.036 psid	+/- 0.057 psid

Absolute Pressure (P)

Calibration - Error Source	1 σ	2 σ
Calibrated Pressure Gages	+/- 0.01 psia	+/- 0.01 psia
Ambient Pressure	+/- 0.005 psia	+/- 0.005 psia
Calibration Curve	+/- 0.006 psia	+/- 0.012 psia
Total Calibration Error	+/- 0.021 psia	+/- 0.027 psia
Measurement Error	**1 σ**	**2 σ**
Set A	+/- 0.032 psia	+/- 0.064 psia
Set B	+/- 0.035 psia	+/- 0.070 psia
Set C	+/- 0.038 psia	+/- 0.076 psia
Total Error	**1 σ**	**2 σ**
Set A	+/- 0.053 psia	+/- 0.085 psia
Set B	+/- 0.056 psia	+/- 0.091 psia
Set C	+/- 0.059 psia	+/- 0.097 psia

APPENDIX B

Calibration Data

Differential Thermocouple (ΔT)

Thermocouple Location TC1/TC2	Measured ΔT (°C)	Thermocouple Output (V)	Predicted ΔT (°C)	Calibration Error (°C)
IP/B	-3.5	-1.93E-04	-3.50	0.00
IP/B	-3	-1.60E-04	-2.93	0.07
IP/B	-2.5	-1.30E-04	-2.42	0.08
IP/B	-2	-1.03E-04	-1.94	0.06
IP/B	-1.5	-7.42E-05	-1.45	0.05
IP/B	-1	-4.44E-05	-0.93	0.07
IP/B	-0.5	-1.58E-05	-0.43	0.07
IP/B	-0.2	5.81E-07	-0.15	0.05
IceP/IceP	0	7.49E-06	-0.03	-0.03
IceP/IceP	0	7.33E-06	-0.03	-0.03
B/IP	0.5	3.44E-05	0.44	-0.06
B/IP	1	6.32E-05	0.93	-0.07
B/IP	1.5	9.23E-05	1.44	-0.06
B/IP	2	1.21E-04	1.93	-0.07
B/IP	2.5	1.50E-04	2.43	-0.07
B/IP	3.1	1.86E-04	3.07	-0.03
B/IP	3.5	2.04E-04	3.38	-0.12
B/IP	4	2.35E-04	3.92	-0.08
B/IP	4.5	2.67E-04	4.47	-0.03
B/IP	5	2.96E-04	4.97	-0.03
B/IP	6	3.54E-04	5.97	-0.03
B/IP	7	4.13E-04	7.00	0.00
B/IP	8	4.73E-04	8.04	0.04
B/IP	9	5.32E-04	9.07	0.07
B/IP	10	5.95E-04	10.15	0.15

IP = Ice point (0°C reference)
B = Warming bath (measured via high accuracy capillary thermometer)

Linear Calibration Curve $y = a + bx$

a = -0.16069 b = 17336.84

y: °C
x: Volts

Differential Pressure Transducer (ΔP)

Measured ΔP (psid)	P2D Output (V)	Predicted ΔP (psid)	Calibration Error (psid)
-2	-1.32E-03	-2.01	-0.0127
-1	-9.25E-04	-1.01	-0.0148
-1	-9.00E-04	-0.95	0.0483
0	-5.20E-04	0.00	0.0006
0	-5.09E-04	0.03	0.0262
0	-5.27E-04	-0.02	-0.0181
0	-5.21E-04	0.00	-0.0027
5	1.49E-03	5.03	0.0344
5	1.48E-03	5.00	-0.0029
10	3.48E-03	10.02	0.0169
10	3.44E-03	9.90	-0.0960
15	5.49E-03	15.03	0.0346
15	5.48E-03	15.02	0.0155
20	7.46E-03	19.98	-0.0238
20	7.46E-03	19.97	-0.0346
25	9.48E-03	25.02	0.0228
25	9.46E-03	24.98	-0.0235
30	1.15E-02	30.02	0.0186
30	1.15E-02	29.99	-0.0107
35	1.35E-02	35.06	0.0592
35	1.35E-02	34.98	-0.0230
40	1.55E-02	39.98	-0.0211
40	1.55E-02	39.99	-0.0053
45	0.017456	45.00	-0.0046
45	0.0174599	45.01	0.0052
50	1.95E-02	50.01	0.0116

Linear Calibration Curve $y = a + bx$

a = 1.3013 b = 2503.102

y: psid
x: Volts

Absolute Pressure Transducer (P)

Measured P (psia)	P1A Output (V)	Predicted P (psia)	Calibration Error (psia)
0.96684	4.16E-04	0.9444	-0.02245
0.96684	4.21E-04	0.9559	-0.01096
3.86736	1.58E-03	3.8611	-0.00627
3.86736	1.58E-03	3.8628	-0.00452
7.73472	3.13E-03	7.7322	-0.00256
7.73472	3.14E-03	7.7411	0.00640
11.60208	4.68E-03	11.5826	-0.01951
11.60208	4.68E-03	11.5845	-0.01756
14.37014	5.79E-03	14.3654	-0.00475
14.37	5.79E-03	14.3722	0.00221
14.37	5.80E-03	14.3841	0.01410
19.370	7.82E-03	19.4407	0.07068
19.370	7.83E-03	19.4563	0.08626
24.370	9.77E-03	24.3018	-0.06821
24.370	9.78E-03	24.3242	-0.04580
29.370	1.18E-02	29.4092	0.03923
29.370	1.18E-02	29.4313	0.06126
34.370	0.0137899	34.3461	-0.02386
34.370	1.38E-02	34.3689	-0.00106
39.370	1.58E-02	39.3392	-0.03080
39.370	1.58E-02	39.3641	-0.00585
44.370	1.78E-02	44.3437	-0.02626
44.370	1.78E-02	44.3652	-0.00483
49.370	1.98E-02	49.3851	0.01510

Linear Calibration Curve $y = a + bx$

a = -0.09554 b = 2497.602

y: psid
x: Volts

APPENDIX C

Fluid Properties

The properties for fluids used in this study were derived from property charts supplied by the respective fluid vendor. The following table shows the properties of the candidate fluids at 11 °C.

Fluid			Ethylene Glycol		FC-72		PAO
Density	ρ	kg/m^3	1123.0		1707.9		797.5
Specific Heat	c_p	J/kg*K	2343.0		1026.3		2173.5
Thermal Conductivity	k	W/m*K	0.2455		0.0587		0.1436
Dynamic Viscosity	μ	$N*s/m^2$	3.279E-02		7.943E-04		0.000E+00

APPENDIX D

Mass Flow and Reynolds Number Calculations

Mass Flow Rate Estimation

Flowmeter telemetry (direct observation)

$\dot{m} \approx$ **4.7 g/sec +/- 1.7 g/sec**

Pump Power Correlation

20% Maximum Pump Speed (4000 rpm) → 800 rpm

High flow rate pump head: 0.94 ml/rev

FC-72 density @ 11_oC: 1707 kg/m^3

$\dot{m} \approx$ **21.4 g/sec +/- 15%**

Set A Data - ΔT Slope

$$\dot{m}c_p = \frac{dq_{in}}{d(\Delta T)} = 4.91 \text{ W/K}$$

FC-72 specific heat @ 11°C, cp = 1026 J/kgK

$\dot{m} \approx$ **4.8 g/sec**

Reynolds Number Calculation

$$\text{Re} = \frac{\dot{m}D_h}{A_c\mu}$$

For: $\dot{m}$ = 4.8 g/sec — Estimated mass flow rate from Set A

D_h = 3.0 mm — Channel Hydraulic Diameter

A_c = 9.28 mm^2 — Channel cross sectional area

μ = 7.94 E-4 Ns/m^2 — FC-72 dynamic viscosity @ 11°C

Re ≈ 1950

APPENDIX E

Procedural Notes

For single-phase fluid testing, a complete loop fill is essential for generating quality data. Air remaining in the system will change the heat transfer characteristics of fluid, cause flow disturbances, and foul flowmeter measurements. Therefore, the loop was filled with process fluid using a vacuum pull method. The steps for filling FC-72 follow:

1) Evacuate entire system, including reservoir, to ~ 1in-Hg
2) Shut reservoir isolation valve, open reservoir top hatch
3) Transfer approximately 3.5 liters of FC-72 into reservoir, close top hatch
4) Evacuate reservoir (using an inline transparent condenser to watch for FC-72 condensation) - approximately 3 in-Hg
5) Close vacuum port at reservoir top before vacuum pump shut off
6) Configure gear pump for low 25% pump speed
7) Open reservoir isolation valve and turn on gear pump
8) Observe loop filling through test section window and clear filter casing

Initially, some void regions will be observed flowing through the test section and in the filter. These void regions should almost entirely disappear as the lower pressure of the reservoir pulls them from the main loop and into the reservoir. Once no bubbles are seen passing the test section window, the reservoir isolation valve may be closed.

Bibliography

1 Ahsmann, G. and R. Kronig. "The Influence of Electric Fields on the Convective Heat Transfer in Liquids," Appied Scientific Research, Vol. A2, pp. 235-244, 1950, Erratum in A3, pp. 85-88 (1951).

2 Allen, P.H.G. "Electric Stress and Heat Transfer." Br. J. Applied. Physics, Vol 10, pp. 347-351 (1959).

3 Bergles, A.E. and R.L. Webb. "Bibliography on Augmentation of Convective Heat and Mass Transfer," Augmentation of Convective Heat and Mass Transfer. Ed. A.E. Bergles and R.L. Webb. New York: ASME, 1970.

4 Chang, J. and A. Watson. "Electromagnetic Hydrodynamics," IEEE Transactions on Dielectrics and Electrical Insulation, Vol. 1, No. 5, pp. 871-895 (October 1994).

5 Davidson, J.H. and F.A. Kulacki. "Convective Heat Transfer with Electric and Magnetic Fields," Handbook of Single-Phase Convective Heat Transfer. Ed. Sadik Kakaç and others. New York: John Wiley & Sons, 1987.

6 Doebelin, Ernest O. Measurement Systems: Application and Design 3rd edition. New York: McGraw-Hill Book Company, 1983.

7 Ebeling, Alvin. Fundamentals of Aircraft Environmental Control. New York: Hayden Book Company, Inc., 1968.

8 Fernandez, J.L. Electrohydrodynamic Enhancement of Forced Convection Heat Transfer in Tubes. Ph.D. thesis, University of Bristol, 1975.

9 Incropera, Frank P. and David P. DeWitt. Fundamentals of Heat and Mass Transfer 4th edition. New York: John Wiley & Sons, 1996.

10 Jones, T.B. "Electrohydrodynamically Enhanced Heat Transfer in Liquids – A Review," Advances in Heat Transfer, Vol. 14, Academic Press, New York, pp.107-148 (1978).

11 Kays, W.M. and A.L. London. Compact Heat Exchngers 3rd edition. New York: McGraw-Hill Book Company, 1984.

12 Levy, E.K. Effects of Electrostatic Fields on Forced Convection Heat Transfer. M.S. thesis, Massachusetts Institute of Technology, Cambridge, Mass., 1969.

13 Mascarenhas, S. "Thermodynamical Theory of Thermal Conduction of Dielectrics Under Electric Fields." Nuovo Cimento, Series B, Vol. 5, pp. 1118-1121 (1957).

14 Ohadi, M.M. Lecture notes, "State of the Art and Emerging Technologies in Enhanced Heat Transfer", University of Maryland-College Park, 18-19 April 1996.

15 Ohadi, M.M., N. Sharaf, and D.A. Nelson. "Electrohydrodynamic Enhancement of Heat Transfer in a Shell-and-Tube Heat Exchanger," Experimental Heat Transfer, Vol. 4, pp.19-39 (1991).

16 Saville, D.A. "Electrohydrodynamics: The Taylor-Melcher Leaky Dielectric Model," Annual Review of Fluid Mechanics, Vol 29, pp.27-64 (1997).

17 Singh, A. Electrohydrodyamic (EHD) Enhancement of In-Tube Boiling and Condensation of Alternate (Non-CFC) Refrigerants. Ph.D. dissertation, University of Maryland, College Park, MD, 1995.

18 The Temperature Handbook Vol. 29. Product Catalog, Omega Engineering Incorporated, Stamford, CT, 1995.

19 Weber, K.H. and G.H. Halsey. "Free Convection in Electric Fields." Proc. Heat Transfer Fluid Mechanics. Institute, No. 19, 1953.

20 Woodson, H.H. and J.R. Melcher. Electromechanical Dynamics. New York: John Wiley and Sons, Inc., 1968.

21 Yabe, A. "Active Heat Transfer Enhancement by Applying Electric Fields," ASME/JSME Thermal Engineering Proceedings, Vol. 3 (1991).

Vita

Captain William T. Caldwell was born on 14 December 1970 in Lexington, Kentucky, and is the son of Thomas A. and Julie G. Caldwell of Campbellsville, Kentucky. He has one brother, Brian T. Caldwell. Captain Caldwell graduated from Taylor County High School in Campbellsville, Kentucky in 1989, and entered the United States Air Force Academy, in Colorado Springs, Colorado. Upon graduation in June 1993, he received a regular commission in the United States Air Force and a Bachelor of Science Degree in Astronautical Engineering. Soon after he graduated, he was married to the former Cami G. Moss, of Campbellsville, Kentucky, his high school sweetheart. Their first assignment was to Cape Canaveral Air Force Station, Florida, where for three years, he served the 45th Space Wing as a Field Program Manager for the Global Positioning System (GPS). In May 1996, he entered the School of Engineering, Air Force Institute of Technology, and upon graduation will be assigned to the National Air Intelligence Center (NAIC) at Wright Patterson Air Force Base, Ohio.

Permanent Mailing Address: 1533 Shiloh Road
Campbellsville, KY 42718

REPORT DOCUMENTATION PAGE

Form Approved
OMB No. 0704-0188

1. AGENCY USE ONLY *(Leave blank)*	2. REPORT DATE	3. REPORT TYPE AND DATES COVERED
	December 1997	Masters Thesis

4. TITLE AND SUBTITLE

Development and Validation of an Experimental Test Rig for Electrohydrodynamic Enhancement of Forced Convective Heat Transfer

5. FUNDING NUMBERS

6. AUTHOR(S)

William T. Caldwell, Capt, USAF

7. PERFORMING ORGANIZATION NAME(S) AND ADDRESS(ES)

Air Force Institute of Technology
2950 P Street
WPAFB OH 45433-7765

8. PERFORMING ORGANIZATION REPORT NUMBER

AFIT/GA/ENY/97D-05

9. SPONSORING/MONITORING AGENCY NAME(S) AND ADDRESS(ES)

Dr. David M. Pratt Phone: (937)255-0251
AFRL/VAVE, Bldg 45 Annex
2130 Eighth Street, Suite 1
WPAFB, OH 45433-7542

10. SPONSORING/MONITORING AGENCY REPORT NUMBER

11. SUPPLEMENTARY NOTES

Maj. Jeffery K. Little, USAF
AFIT/ENY
Phone: (937) 255-3636x4723 Email: jlittle@afit.af.mil

12a. DISTRIBUTION/AVAILABILITY STATEMENT

Approved for public release; distribution unlimited

12b. DISTRIBUTION CODE

A

13. ABSTRACT *(Maximum 200 words)*

This report details the development of a facility for the experimental investigation of electrohydrodynamic (EHD) enhancement of forced convection heat transfer. The test facility was developed for the Thermal and Transparencies Laboratory (TATLAB), Air Force Research Laboratory (AFRL), for use in future research into the applicability of EHD for the miniaturization of Air Force heat exchangers. During this research, a closed loop, medium scale electrohydrodynamic test rig was developed and brought online. The test fluid loop was integrated with a data acquisition and parameter control system. Basic loop and fluid performance testing was accomplished through the use of a 3mm hydraulic diameter, square channel test section using Flourinert FC-72, a dielectric electronics coolant, as the working fluid. Due to the design of the test section, no heat transfer data was generated in this initial study. However, this study greatly expanded the experimental and practical understanding of the EHD phenomenon within AFRL, by providing a working knowledge of the basics of effective EHD test section design, contamination control procedures, and loop design and operation. Deficiencies in the design of the loop, data acquisition system, and test section were identified and recommendations for improvements in future work were delivered. The Air Force Research Laboratory is now poised to generate useful EHD heat transfer data with this test facility.

14. SUBJECT TERMS

Electrohydrodynamics, Convective Heat Transfer, Experimental Facility Development, Heat Transfer Enhancement, Heat Exchanger

15. NUMBER OF PAGES

106

16. PRICE CODE

17. SECURITY CLASSIFICATION OF REPORT	18. SECURITY CLASSIFICATION OF THIS PAGE	19. SECURITY CLASSIFICATION OF ABSTRACT	20. LIMITATION OF ABSTRACT
Unclassified	Unclassified	Unclassified	UL